haematologica
Journal of the Ferrata Storti Foundation

Different inflammatory, fibrotic, and immunologic signatures between pre-fibrotic and overt primary myelofibrosis

by Seung-Hyun Jung, Sung-Eun Lee, Sujin Yun, Da-Eun Min, Youngjin Shin, Yeun-Jun Chung and Sug Hyung Lee

Received: April 12, 2024.
Accepted: September 27, 2024.

Citation: Seung-Hyun Jung, Sung-Eun Lee, Sujin Yun, Da-Eun Min, Youngjin Shin, Yeun-Jun Chung and Sug Hyung Lee. Different inflammatory, fibrotic, and immunologic signatures between pre-fibrotic and overt primary myelofibrosis.
Haematologica. 2024 Oct 10. doi: 10.3324/haematol.2024.285598 [Epub ahead of print]

Different inflammatory, fibrotic, and immunologic signatures between pre-fibrotic and overt primary myelofibrosis

Seung-Hyun Jung[1,2,3,†,*], Sung-Eun Lee[4,†], Sujin Yun[3], Da-Eun Min[1], Youngjin Shin[5], Yeun-Jun Chung[2,3,5,6,*], Sug Hyung Lee[3,7,8,*]

Departments of [1]Biochemistry, [2]Precision Medicine Research Center/Integrated Research Center for Genome Polymorphism, [3]Medical Sciences, [4]Internal Medicine, [5]Basic Medical Science Facilitation Program, [6]Microbiology, [7]Cancer Evolution Research Center, and [8]Pathology, College of Medicine, The Catholic University of Korea, Seoul, South Korea

[†]These authors contributed equally to this work

Running title: Single-cell transcriptome of primary myelofibrosis

***Correspondence to:**

Sug Hyung Lee, Department of Pathology, College of Medicine, The Catholic University of Korea, 222 Banpo-daero, Seocho-gu, Seoul 06591, Republic of Korea. E-mail: suhulee@catholic.ac.kr, or

Yeun-Jun Chung, Department of Microbiology, College of Medicine, The Catholic University of Korea, 222 Banpo-daero, Seocho-gu, Seoul 06591, Republic of Korea. E-mail: yejun@catholic.ac.kr, or

Seung-Hyun Jung, Department of Biochemistry, College of Medicine, The Catholic University of Korea, 222 Banpo-daero, Seocho-gu, Seoul 06591, Korea, E-mail: hyun@catholic.ac.kr

Keywords: myeloproliferative neoplasm, pre-fibrotic myelofibrosis, overt myelofibrosis, single-cell RNA sequencing, hematopoietic stem and progenitor cell, megakaryocyte

Funding

This study was supported by grants from National Research Foundation of Korea (2017R1A2B2002314, 2019R1A5A2027588, 2017R1E1A1A01074913, RS-2022-00165497, RS-2024-00450891, and 2019R1C1C1004909).

Acknowledgments

We also appreciate the support by Basic Medical Science Facilitation Program through the Catholic Medical Center of the Catholic University of Korea funded by the Catholic Education Foundation, and KREONET (Korea Research Environment Open NETwork), which is managed and operated by KISTI (Korea Institute of Science and Technology Information).

Authorship

SHJ, SEL, YJC, and SHL wrote the manuscript. YJC, SEL, and SHL conceived and designed the study. SHJ, SY, DEM and SEL participated in acquisition of data, sample preparation and clinical reviews. SHJ and YS carried out the bioinformatics analysis. All authors read and approved the final manuscript.

Data Availability

Raw sequencing data generated for scRNA-seq have been deposited in Sequence Read Archive under accession number PRJNA1070224.

Disclosure of Potential Conflicts of Interest

The authors declare no competing financial interests.

Abstract

Primary myelofibrosis (PMF) is a myeloid proliferative neoplasm (MPN) characterized by bone marrow (BM) fibrosis. Pre-fibrotic PMF (pre-PMF) progresses to overt PMF. Megakaryocytes (MKs) play a primary role in PMF; however, the functions of MK subsets and those of other hematopoietic cells during PMF progression remain unclarified. Therefore, we analyzed BM aspirates in pre-PMFs, overt PMFs, and other MPNs using single-cell RNA sequencing (scRNA-seq). We identified 14 cell types with subsets, including hematopoietic stem and progenitor cells (HSPCs) and MKs. HSPCs in overt PMF were MK-biased and inflammation/fibrosis-enriched. Among MKs, the epithelial-mesenchymal transition (EMT)-enriched subset was abruptly increased in overt PMF. MKs in non-fibrotic/non-PMF MPN were MK differentiation-enriched, whereas those in fibrotic/non-PMF MPN were inflammation/fibrosis-enriched. Overall, the inflammation/fibrosis signatures of the HSPC, MK, and $CD14^+$ monocyte subsets increased from pre-PMF to overt PMF. Cytotoxic and dysfunctional scores also increased in T and NK cells. Clinically, MK and HSPC subsets with high inflammation/fibrosis signatures were frequent in the patients with peripheral blood blasts ≥1%. scRNA-seq predicted higher cellular communications of MK differentiation, inflammation/fibrosis, immunologic effector/dysfunction, and tumor-associated signaling in overt PMF than pre-PMF. However, no decisive subset emerged during PMF progression. Our study demonstrated that HSPCs, monocytes, and lymphoid cells contribute to PMF progression, and subset specificity existed regarding inflammation/fibrosis and immunologic dysfunction. PMF progression may depend on multiple cell types' alterations, and EMT-enriched MKs may be potential targets for the diagnosis and therapy of the progression.

Introduction

Philadelphia-negative myeloproliferative neoplasm (MPN) is a myeloid hematopoietic stem cell (HSC) neoplasm characterized by the overproduction of myeloid, erythroid, and megakaryocytic (MK) cells, resulting in polycythemia vera (PV), essential thrombocythemia (ET), and primary myelofibrosis (PMF).[1] PV, ET, and PMF share the clinical and molecular features that may result in disease progression to acute myeloid leukemia and harbor specific driver mutations (*JAK2, CALR,* or *MPL*) that activate JAK2 signaling.[2] The major criteria for diagnosing PMF include MK proliferation with bone marrow (BM) fibrosis, the absence of diagnostic criteria for ET or PV, and the presence of driver mutations or additional high-molecular-risk mutations.[3-5] JAK inhibitors can relieve symptoms in PMF but do not entirely resolve BM fibrosis,[6] suggesting that the pathogenesis of PMF is more complex than those of other MPNs.[7]

PMF arises from a single HSC with driver mutations that endow it with a selective advantage, thereby promoting myeloid cell proliferation and BM fibrosis.[8] Atypical MKs are the histological hallmark of PMF and play a vital role in its development.[4] PMF-MKs are characterized by the enrichment of inflammatory and immunoregulatory signals that alter cross-talks between BM cells, thereby exacerbating genetic instability in PMF-HSCs[9, 10] and promoting fibrosis.[5, 10] However, the specific MK subsets relevant to PMF remain undetermined. Furthermore, the contribution of other myeloid cells, besides MK, to PMF is largely uncharacterized. Immune evasion and dysregulation of the immune system contribute to the clonal evolution of PMF-HSCs and BM fibrosis.[11-13] These immunologic alterations have been identified in the peripheral blood (PB) cells of patients with PMF; however, they do not reflect the complete immunologic landscape of PMF-BM.

The 2016 WHO classification categorizes PMF into pre-fibrotic PMF (pre-PMF, grade 0 or

1 fibrosis) and overt PMF (overt PMF, grade 2 or 3 fibrosis).[3] As constitutional symptoms and hematologic pathology worsen, pre-PMF progresses to overt PMF, resulting in poorer survival.[3, 14-16] Subtle genomic differences in the hematopoietic clones (unfavorable karyotypes and high-molecular-risk mutations) and bulk transcriptomic differences in inflammatory signatures have been noted between pre-PMF and overt PMF.[14-16] However, the precise molecular mechanisms underlying the progression from pre-PMF to overt PMF remain unexplored.

JAK-STAT activation has been identified as a driver mechanism for MPNs; nevertheless, PMF remains the most heterogeneous disease among MPNs and is further complicated by coexisting inflammation.[17] After acquiring the driver mutations, PMF presents with decades of latency before developing disease manifestations.[18] These studies suggest the existence of multiple disease-modifying factors that could result in diverse cell states or subpopulations in the BM cells of patients with PMF.

Single-cell RNA sequencing (scRNA-seq) can define the individual transcriptomes of admixed cells in tissues, further dissecting subpopulations and enabling precise inference of the functions and interactions of the cells that cannot be distinguished by traditional bulk analyses.[19] To the best of our knowledge, only a handful of the scRNA-seq datasets for PMF-BM are currently available. A patient with overt PMF was assessed using a BM biopsy, with primary analyses of non-hematopoietic cells.[10] Furthermore, PMFs were studied by simultaneous mutation and scRNA-seq analyses; however, this proof-of-principle method utilized in that study could not intersect multiple phenotypic readouts across a range of cell subtypes,[20] warranting further investigations.

In this study, we hypothesized that specific cell subtypes, besides MK, might exist in overt PMF, and that their distinctive molecular signatures might contribute to PMF progression. To elucidate these, we analyzed BM aspirates from pre-PMF and overt PMF using scRNA-seq

and identified cellular subpopulations with inflammatory, fibrotic, and immunologic signatures between pre-PMF and overt PMF.

Methods

Bone marrow samples

BM aspirates were collected from 33 patients with MPN (five with ET, one with PV, five with pre-PMF, 12 with overt PMF, six with post-ET-MF, and four with post-PV-MF). Among the 12 patients with overt PMF, six were treated with the JAK inhibitor ruxolitinib, while the remaining six were not treated with any JAK inhibitor. To minimize the risk of PB dilution in BM aspirate samples, we repeated the aspiration at a different site if a dry tap was encountered during the procedure. We also performed microscopic examination of the BM aspirates to assess their quality and composition. The patients' BM fibrosis was confirmed using BM biopsies, indicating that our aspirates represented the remaining fluidic areas surrounding the fibrotic PMF-BM. This study was approved by the institutional review board of the Catholic University of Korea (KC20TISI0206).

scRNA-seq library preparation

Individual cells in BM aspirates were isolated using density gradient centrifugation with a Ficoll-Paque Plus medium (GE Healthcare). After removing red blood cells (RBCs) using RBC lysis buffer (Miltenyi Biotec), the cells were counted and stored at −80°C until their utilization. The scRNA-seq library was prepared using the Chromium instrument system with a Single Cell 3’ v3 Reagent kit (10x Genomics), according to the manufacturer’s protocol. scRNA-seq libraries were sequenced on the Illumina NovaSeq platform. Raw sequencing data have been deposited in Sequence Read Archive under accession number PRJNA1070224. Additional details of the scRNA-seq library preparation are described in the Supplementary Methods.

scRNA-seq data analyses

The sequenced data were processed into expression matrices using CellRanger (10x Genomics). Sequencing reads were mapped to the GRCh38 reference genome. Bioinformatics processing of the scRNA-seq data was performed using Seurat.[21] After removing low-quality cells, the data was log-normalized, and highly variable features were identified based on a variance stabilizing transformation method. All individual datasets were integrated using Harmony.[22] Principal components analysis and graph-based clustering were performed on the integrated datasets, and the clustering data were applied to the uniform manifold approximation and projection. Each cell cluster was annotated for its cell type using SingleR and well-known cell-type-specific markers.

Differentially expressed gene (DEG) analysis was used to identify significant DEGs within each cluster using the 'FindMarkers' function in Seurat. Gene signature scores were calculated using UCell. Gene set enrichment analysis (GSEA) was performed using fgsea with MSigDB. Single-cell reference mapping compared the MK subset abundance between PMF and other MPNs. Receptor-ligand interactions were analyzed using CellChat to examine cell-to-cell communication between different cell types in PMF-BM.[23] Additional details of the scRNA-seq data analyses are provided in the Supplementary Methods.

Statistical analysis

Fisher's exact test was used for categorical variables. The Mann–Whitney U test was used for continuous variables. Statistical analyses were performed using SPSS (IBM). GraphPad Prism software was used to create graphs. Statistical significance was set at p-value < 0.05 for all the analyses.

Results

BMs of overt PMF patients are enriched with MKs and HSPCs

We performed scRNA-seq on whole BM mononuclear cells (BM-MNCs) isolated from 17 patients with PMF (five with pre-PMFs and 12 with overt PMFs) (Table 1). After quality control, we obtained 98,677 cells from pre-PMF (19,452 cells) and overt PMF (79,215 cells) clustered in 14 cell populations: hematopoietic stem and progenitor cell (HSPC), MK, erythroid cell, five myeloid lineages [$CD14^+$ monocyte, $CD16^+$ monocyte, myeloid dendritic cell (mDC), plasmacytoid dendritic cell (pDC), and neutrophil], five lymphoid lineages [T cell, NK cell, pre-B cell, B cell, and plasma cell (PC)], and mesenchymal stromal cell (MSC) (Figure 1A).

We observed differences in the abundance of cells between pre-PMF and overt PMF. In overt PMF, we found increased HSPCs (9.3% of BM-MNCs) and MKs (11.7%), compared to pre-PMF (HSPCs: 3.4%, MKs: 5.9%) (Figure 1B-D). However, these differences were not statistically significant. On the other hand, the populations of mDC, neutrophils, and PCs significantly decreased as the diseases progressed (Figure 1D). Regarding clinical variables, MKs and HSPCs were enriched in the BM of patients with PMF with PB blasts ≥1% compared to those with PB blasts <1% (MK: 16.2% vs 4.5%, $P = 0.015$; HSPC: 12.4% vs 3.3%, $P = 0.027$). MKs were also enriched in the BM of patients at high risk according to the Mutation-enhanced International Prognostic Score System (MIPSS) compared to those at low or intermediate risk (11.5% vs 4.2%, $P = 0.021$). In line with a previous finding,[24] it was observed that lymphocyte levels decreased in patients treated with ruxolitinib compared to those not treated. We found no significant differences in cell type abundance according to the PMF driver mutations, age, leukocyte count, hemoglobin count, platelet count, or prognostic groups of the IPSS and Dynamic IPSS-plus (DIPSS-plus). Taken together, the BM cellular

abundance of HSPCs and MKs is noted during PMF progression and associated with an increase in PB blasts.

HSPCs in overt PMF are MK-biased with inflammatory and fibrotic activation

The sub-clustering of HSPC revealed nine subsets (Figure 2A; Supplementary Table S1): HSC (HSC1 and HSC2 expressing *AVP* and *HLF*), MK-erythroid-mast progenitor (MEMP expressing *CLC* and *FCER1A*), MK-erythroid progenitor (MEP1 and MEP2 expressing *GATA1* and *KLF1*), early erythroid (expressing *ALAS2* and *GYPA*), granulocyte-monocyte progenitor (GMP expressing *MPO* and *AZU1*), lymphoid progenitor (expressing *CD247* and *THEMIS*), and proliferating cell (expressing *TOP2A* and *MKI67*).

In HSC1, GSEA identified the enrichment of inflammatory (tumor necrosis factor α signaling and interferon-gamma response) and fibrotic signaling [transforming growth factor β (TGF-β) and coagulation] (Supplementary Figure S1A). Pseudo-bulk DEG analysis identified eight overt PMF-specific genes, of which *BACH2*, *ANXA2*, and *ANO2* were associated with MK differentiation (Supplementary Figure S1B; Supplementary Table S2).[25] The abundance of HSC1 was not different between pre-PMF and overt PMF (Figure 2B), suggesting that HSC1 might be related to PMF development.

The MEP1 subset was abundant in overt PMF compared to pre-PMF (11.0% vs 4.2%, P = 0.029) (Figure 2B). Additionally, MEP1 was more abundant in patients with PMF with PB blasts ≥1% compared with those with PB blasts <1% (13.6% vs 4.1%, P = 0.001). GSEA of MEP1 revealed enrichment in the MK-lineage differentiation (Supplementary Figure S1C).[26] Eight overt PMF-specific DEGs were detected in MEP1 (Supplementary Figure S1D; Supplementary Table S2). There were no differences in HSC1 and MEP1 between the ruxolitinib-exposed and unexposed patients, in terms of quantitative or qualitative (inflammatory and fibrotic signaling) measures (Supplementary Figure S1E).

Previously, MK-biased HSPCs expressing *PF4*, *MPIG6B*, *VWF*, *SELP*, and *GP9* were observed in the PB of patients with PMF.[5] In our study, the proportions of these HSPCs were higher in overt PMF than in pre-PMF (27.7% vs 8.3%, $P = 3.7x10^{-99}$) (Figure 2C). Notably, the MK signatures were not limited to a specific HSPC subset, suggesting that the MK bias may be widespread among HSPCs (Figure 2C; Supplementary Figure S2). *MPIG6B* and *PF4* expressions were observed in uncommitted (HSC1 and HSC2) and lineage-committed subsets (MEP1 and MEP2) (Figure 2D), consistent with a previous report.[5] The HSPCs expressing *MPIG6B* (59.6% vs 28.9%, $P = 1.7x10^{-81}$) and *PF4* (22.0% vs 10.7%, $P = 1.5x10^{-16}$) were more prevalent in overt PMF than in pre-PMF (Supplementary Figure S2). Collectively, HSC1 and MEP1 subsets in overt PMF show a higher bias toward MK production compared to pre-PMF. These subsets may have a preference for expanding or interacting with other BM cells to promote MK differentiation, and BM inflammation and fibrosis.

Increased inflammation and fibrosis signatures in MKs of overt PMF

We identified five MK subsets (MK1–5; Figure 3A; Supplementary Table S1). The proportion of MK5 was higher in overt PMF than in pre-PMF (Figure 3B). We compared the module scores to identify the quality difference among the MK subsets and found that MK differentiation, fibrosis, TGF-β, and cytokine scores increased from pre-PMF to overt PMF (Figure 3C). These signatures increased in overt PMF of all MK subsets, except MK2. Notably, MK5 was most specific to overt PMF and was scarce in pre-PMF (1.3% vs 0.2%, $P = 0.044$) (Figure 3B). Furthermore, the MK5 subset was enriched in patients with PMF with PB blasts ≥1% compared with those with PB blasts <1% (2.0% vs 0.12%, $P = 8.2x10^{-5}$). MK5 specifically expressed epithelial-mesenchymal transition (EMT)-related genes, including *TTK*, *ITGA6*, and *ILK* (Supplementary Figure S3A).[27] There were no significant

differences in MK subsets between the patients exposed to ruxolitinib and those who were not exposed (Supplementary Figure S3B-C).

We performed a pseudo-bulk DEG analysis on all MK cells and identified 19 overt PMF-specific DEGs (Figure 3D; Supplementary Table S2). Up-regulated genes, including *COL24A1*, *CXCL2*, and *LTBP1*, were related to fibrosis and enriched in the MK3 subset. For example, *CXCL2*, which is known to be associated with pulmonary fibrosis,[28] was nearly absent in pre-PMF but was highly expressed in MK3 of overt PMF (0.9% vs 10.9% of MK, $P = 2.3x10^{-12}$). *LTBP1* is an extracellular matrix protein associated with fibrillin-microfibrils[29] and can induce TGF-β activation,[30] which is essential for fibrosis development in PMF.[31] *LTBP1* expression increased with the progression from pre-PMF to overt PMF (15.7% vs 38.9%, $P = 7.8x10^{-28}$).

Furthermore, we projected the MKs from 16 patients with non-PMF MPN (five with ET, one with PV, six with post-ET-MF, and four with post-PV-MF) onto those from patients with PMF to compare MK subset differences among MPNs. Most MK cells (96.6%) in the ET/PV cases were assigned to the MK2 subset. In contrast, the MK subset distribution of post-ET/PV-MF was widespread and similar to those of PMF (Supplementary Figure S3D). Notably, MK5, the most overt PMF-specific subset, showed a similarly high distribution between overt PMF and post-ET/PV-MF (Supplementary Figure S3E). Collectively, scRNA-seq identified MK5 as the most overt PMF-specific subset with an increased fibrosis signature.

Overt PMF immune cells show immune dysfunction and suppression signatures

We identified 15 subsets of T and NK cells in the BM aspirates (Figure 4A–B; Supplementary Table S1): naïve T ($CD8^+$, $CD4^+$, and $CD3^-CD4^+$), helper T, regulatory T (Treg), mucosal-associated invariant T (MAIT), γδ T, cytotoxic memory (Tmem), cytotoxic

terminal effector (Teff), $CD56^{bright}$ NK, NK (NK1, NK2, NK3, and NK4), and proliferating cell subsets. The subset distribution of T and NK was not significantly different between pre-PMF and overt PMF, nor between ruxolitinib-exposed and unexposed patients, except for NK1: the NK1 subset significantly decreased in the ruxolitinib-exposed patients (P = 0.009; Supplementary Figure S4A). However, functional module analyses showed a significant increase in cytotoxic scores in most T cell subsets with the progression from pre-PMF to overt PMF (Figure 4C). Similarly, the dysfunctional module score of T cell activation, measured using *PDCD1*, *LAG3*, *TIGIT*, *CD244*, and *CTLA4* expression analyses, increased in the γδ T and Teff subsets with the progression (Supplementary Figure S4B). For example, overt PMF exhibited a higher prevalence of *LAG3*-expressed Teff cells than pre-PMF (P = 0.004) (Figure 4D). These were not significantly different according to the ruxolitinib exposure.

We identified eight $CD14^{+}$ monocyte subsets among the myeloid lineages (Figure 5A–B; Supplementary Table S1). Of these subsets, mono3 increased from pre-PMF to overt PMF (24.5% vs 31.7% of $CD14^{+}$ monocytes) (Figure 5C). Mono3 may be a variant of monocytic myeloid-derived suppressor cell (M-MDSC)[32] that has immunosuppressive functions. Mono3 expressed M-MDSC markers[32] with higher MHC-II expression than that of conventional M-MDSC (Figure 5B). Furthermore, we discovered that the interferon signature in overall $CD14^{+}$ monocytes was significantly higher in overt PMF than pre-PMF ($P = 5.9 \times 10^{-131}$) (Figure 5D). The scRNA-seq analysis revealed altered immune and inflammatory signaling in overt PMF compared to pre-PMF, potentially leading to reduced immune activity.

Prediction of cell-cell communication

Ligand-receptor (LR) interaction analysis using scRNA-seq revealed a higher number and strength of LR interactions in overt PMF than in pre-PMF (Supplementary Figure S5A).

Among the 90 putative interactions identified, 38 were significantly enriched in overt PMF, with 10 exclusive interactions (Figure 6). The difference in interactions between pre-PMF and overt PMF was primarily due to the increased interactions among HSPCs, MKs, T cells, and monocytes (Supplementary Figure S5B), which were identified as overt-PMF-driving cells using scRNA-seq. Overt-PMF-enriched interactions were largely categorized into four signatures (Supplementary Figure S6): MK differentiation (GP1BA and VWF),[5] pro-inflammatory/fibrotic signaling (CD34, CD40, EPHB, and TGF-β)[19, 31, 33, 34], immunologic effector/dysfunction signaling (PROS, SN, THBS, TIGIT, LCK, CCL, and PARs)[35-37], and tumor-associated signaling (ESAM, JAM, and HSPG)[38, 39].

Ephrins and Eph receptors are known mediators of fibrosis.[34] MK3 was identified as the most prominent source of the ephrin ligand (*EFNB2*) in overt PMF, affecting T cells (Supplementary Figure S6). This interaction was not observed in pre-PMF. CD34 and CD40 signaling, which are known to be involved in inflammatory disease development,[19, 33] were exclusively identified in overt PMF (Figure 7A and 7C). MK2 interacted with HSPCs, M-MDSC, and mDC through the *TGFB1*-(*TGFBR1*+*TGFBR2*) axis in pre-PMF (Figure 7B). MK5 strongly expressed *TGFB1*, and HSPCs strongly expressed *ACVR1*, another receptor of the TGF-β signaling, in overt PMF (Figure 7C). This prediction suggests that the *TGFB1*-(*TGFBR1*+*TGFBR2*) axis is activated in pre-PMF, with MK2 as a hub, whereas the *TGFB1*-(*ACVR1*+*TGFBR1*) axis is activated in overt PMF, with MK5 as a hub (Supplementary Figure S7). TIGIT, a marker of T cell exhaustion,[40] inhibits immune cell responses at multiple steps of the tumor□immunity cycle. TIGIT signaling in pre-PMF was predicted to originate from Tmem, whereas that in overt PMF was predicted to originate from Tmem and Treg (Supplementary Figure S6). T cell communication partners in TIGIT signaling were much more diverse in overt PMF than those in pre-PMF, primarily targeting HSPCs and MK3 (Figure 7C).

Discussion

Previous investigations of the molecular pathogenesis in PMF primarily relied on MK alterations. This informational gap led us to analyze pre-PMF, overt PMF, and other MPNs (ET/PV) using scRNA-seq. Our results indicated that the differences between pre-PMF and overt PMF were attributed to the inflammation/fibrosis and immunologic alterations of multiple cellular subsets, rather than one or two. First, specific subpopulations of HSPC, MK, monocyte, and lymphoid cells increased during the progression from pre-PMF to overt PMF. Second, pro-inflammatory/fibrotic and immunologic dysfunction signatures increased during the progression. Third, no single decisive subpopulation emerged during the progression of pre-PMF to overt PMF. These gradual alterations support the idea that pre-PMF and overt PMF are in a disease continuum, with many disease-progressing factors involved in the pathogenesis.

DIPSS-plus system uses eight prognostic survival factors of patients with PMF, including age >65 years, constitutional symptoms, and PB blasts ≥1%.[41] PB blast increase is directly associated with leukemic transformation, plausibly indicating poor survival; however, other possibilities have remained uncertain. Approximately 20% of patients with PMF die from leukemic transformation, with most of them succumbing to BM failure and other complications.[42] We found that the PB blast ≥1% predictor was related to the increase in HSPCs and MKs in PMF-BM, particularly in MEP1 and MK5 subsets. MEP1 was significantly enriched in overt PMF, with a corresponding increase in inflammatory and fibrotic functions. MK5 highly expressed EMT-related genes in our data. EMT and inflammation cooperate in the progression of organ fibrosis.[43] EMT is identified as a hallmark signature of murine PMF,[44] indicating that the PB blast ≥1% predictor may be associated with inflammation and fibrosis in PMF. These data suggest that the blast increase

may result from HSPC and MK proliferation in PMF-BM, which is related to non-leukemic hematologic complications rather than the leukemic transition itself.

Somatically mutated MKs induce or alter the development and progression of MPNs, where MK-derived TGF-β plays a primary role in HSC proliferation and BM fibrosis.[31] Consistent with this, we observed increased TGF-β signaling in overt PMF compared with pre-PMF, particularly owing to high *TGFB1* expression in MK5. MKs are essential in MPN pathogeneses; however, how MKs differ between yet-to-be-fibrotic ET/PV and PMF and between PMF and post-ET/PV-MF remains unclear. In our data, overt PMF exhibited a much higher proportion of MK5 than pre-PMF, with a higher expression of the TGF-β signature. Moreover, non-fibrotic ET/PV revealed lower MK5 abundance than PMF, whereas post-ET/PV-MF showed a similar MK5 abundance to overt PMF. These findings suggest that MK5 may be one of the key determiners in the development and progression of BM fibrosis, irrespective of MPN subtypes.

Dysregulation of the immune system contributes to the expansion and survival of the neoplastic myeloid clone in MPNs.[13] For example, differentiation of monocytes to dendritic cells is reduced in PB, whereas MDSCs increase in PMF.[11, 45] Furthermore, reductions in $CD56^{bright}$ NK cells and $CD3^{+}$ T cells and an increase in Treg cells have been reported in MPNs.[12, 46] However, our study did not identify altered NK or T cell distribution in PMF-BM samples. Instead, we observed increased cytotoxicity and dysfunction scores in the T cell subpopulations of overt PMF. LR pair analysis showed that TIGIT (*TIGIT-NECTIN2* axis) and PARs (mainly *GZMA-F2R* and *GZMA-PARD3* axes) harboring NK and T cell suppressive functions were highly expressed in the cytotoxic cells of PMF interacting with HSPCs. Furthermore, we observed an increase of M-MDSC (immune-suppressive) in myeloid cells in overt PMF. These results indicate that the PMF-BM microenvironment alters

the immune and inflammatory responses of T cells and monocytes, which may lead to reduced immune activities in the BM of PMF.

JAK inhibitors targeting mutant hematopoietic clones have improved the symptoms, splenomegaly, and survival of patients with PMF. However, these drugs are not capable of curing progressed PMF, particularly when used as monotherapy.[47] Inflammation and fibrosis are drivers of PMF pathogenesis; therefore, novel drugs targeting these factors, along with immune modulation, are currently being investigated in clinical trials.[17] In this sense, our molecular data may precisely identify target subpopulations and molecules, enabling the combination of targeted therapy with JAK inhibitors.

Simultaneous BM aspirate and biopsy analysis is essential to precisely delineate the interactions between stromal cells and hematopoietic cells in the BM. However, our study focused on BM aspirates, primarily owing to the challenges of obtaining simultaneous BM biopsies suitable for scRNA-seq. Consequently, the analysis of non-hematopoietic BM cells involved in PMF, such as fibroblasts and myofibroblasts, was precluded. There is a likelihood that the BM aspirates were hemodiluted with contributions from the PB, likely due to extramedullary hematopoiesis. Current consensus suggests that extramedullary hematopoiesis in PMF results from the sequestration, accumulation, and proliferation of circulating progenitor cells.[48, 49] Thus, even with hemodilution, the aspirates would still reflect the neoplastic nature of the BM in PMF patients. However, the impact of extramedullary hematopoiesis on the BM microenvironment in PMF requires further investigation. Second, our study was limited by the complexity of treatments received by the patients, influenced by the rarity of the disease, its broad spectrum, and the variability of therapeutic options. Many overt PMF patients in our study were treated with a JAK inhibitor (ruxolitinib), which would be expected to alter the inflammatory signaling in these patients. However, our findings in overt PMF were predominantly due to PMF progression rather than ruxolitinib treatment. The

small sample size may have led to an underestimation of the impact of ruxolitinib treatment. Therefore, further studies using extended serial BM sampling in a larger cohort of uniformly treated patients are necessary to identify preventive and therapeutic targets for PMF. Additionally, the scRNA-seq methodology we employed did not allow genotyping of driver mutations; therefore, the observed differences between pre-PMF and overt PMF could actually be due to the size of the mutated clones. Finally, there were no BM aspirate controls from healthy individuals.

In summary, our study revealed the single-cell transcriptome signatures and cellular subsets of MK, HSPC, and immune cells, characterized according to PMF progression. However, no overt PMF-specific cell subset emerged during the progression. PMF progression may rely on multiple cell type alterations. MKs, HSPCs, monocytes, and lymphoid cells contributed to the progression, and subset specificity existed regarding inflammation/fibrosis and immunologic dysfunction. Our results may aid in defining the molecular diagnosis for PMF progression and discovering potential target subsets in PMF, such as the EMT-enriched MK5 subset.

References

1. Harrison CN, McLornan DP. Current treatment algorithm for the management of patients with myelofibrosis, JAK inhibitors, and beyond. Hematology Am Soc Hematol Educ Program. 2017;2017(1):489-497.
2. Maslah N, Benajiba L, Giraudier S, Kiladjian JJ, Cassinat B. Clonal architecture evolution in Myeloproliferative Neoplasms: from a driver mutation to a complex heterogeneous mutational and phenotypic landscape. Leukemia. 2023;37(5):957-963.
3. Guglielmelli P, Pacilli A, Rotunno G, et al. Presentation and outcome of patients with 2016 WHO diagnosis of prefibrotic and overt primary myelofibrosis. Blood. 2017;129(24):3227-3236.
4. Arber DA, Orazi A, Hasserjian R, et al. The 2016 revision to the World Health Organization classification of myeloid neoplasms and acute leukemia. Blood. 2016;127(20):2391-2405.
5. Psaila B, Wang G, Rodriguez-Meira A, et al. Single-Cell Analyses Reveal Megakaryocyte-Biased Hematopoiesis in Myelofibrosis and Identify Mutant Clone-Specific Targets. Mol Cell. 2020;78(3):477-492.e8.
6. Schieber M, Crispino JD, Stein B. Myelofibrosis in 2019: moving beyond JAK2 inhibition. Blood Cancer J. 2019;9(9):74.
7. Palandri F, Breccia M, Bonifacio M, et al. Life after ruxolitinib: Reasons for discontinuation, impact of disease phase, and outcomes in 218 patients with myelofibrosis. Cancer. 2020;126(6):1243-1252.
8. Delhommeau F, Dupont S, Tonetti C, et al. Evidence that the JAK2 G1849T (V617F) mutation occurs in a lymphomyeloid progenitor in polycythemia vera and idiopathic myelofibrosis. Blood. 2007;109(1):71-77.
9. Leiva O, Ng SK, Chitalia S, Balduini A, Matsuura S, Ravid K. The role of the extracellular matrix in primary myelofibrosis. Blood Cancer J. 2017;7(2):e525.
10. Leimkuhler NB, Gleitz HFE, Ronghui L, et al. Heterogeneous bone-marrow stromal progenitors drive myelofibrosis via a druggable alarmin axis. Cell Stem Cell. 2021;28(4):637-652.e8.
11. Romano M, Sollazzo D, Trabanelli S, et al. Mutations in JAK2 and Calreticulin genes are associated with specific alterations of the immune system in myelofibrosis. Oncoimmunology. 2017;6(10):e1345402.

12. Wang JC, Sindhu H, Chen C, et al. Immune derangements in patients with myelofibrosis: the role of Treg, Th17, and sIL2Ralpha. PLoS One. 2015;10(3):e0116723.
13. Strickland M, Quek L, Psaila B. The immune landscape in BCR-ABL negative myeloproliferative neoplasms: inflammation, infections and opportunities for immunotherapy. Br J Haematol. 2022;196(5):1149-1158.
14. Finazzi G, Vannucchi AM, Barbui T. Prefibrotic myelofibrosis: treatment algorithm 2018. Blood Cancer J. 2018;8(11):104.
15. Carobbio A, Guglielmelli P, Rumi E, et al. A multistate model of survival prediction and event monitoring in prefibrotic myelofibrosis. Blood Cancer J. 2020;10(10):100.
16. Hussein K, Brakensiek K, Buesche G, et al. Different involvement of the megakaryocytic lineage by the JAK2 V617F mutation in Polycythemia vera, essential thrombocythemia and chronic idiopathic myelofibrosis. Ann Hematol. 2007;86(4):245-253.
17. Baumeister J, Chatain N, Sofias AM, Lammers T, Koschmieder S. Progression of Myeloproliferative Neoplasms (MPN): Diagnostic and Therapeutic Perspectives. Cells. 2021;10(12):3551.
18. Sousos N, Ni Leathlobhair M, Simoglou Karali C, et al. In utero origin of myelofibrosis presenting in adult monozygotic twins. Nat Med. 2022;28(6):1207-1211.
19. Wong WJ, Baltay M, Getz A, et al. Gene expression profiling distinguishes prefibrotic from overtly fibrotic myeloproliferative neoplasms and identifies disease subsets with distinct inflammatory signatures. PLoS One. 2019;14(5):e0216810.
20. Rodriguez-Meira A, Buck G, Clark SA, et al. Unravelling Intratumoral Heterogeneity through High-Sensitivity Single-Cell Mutational Analysis and Parallel RNA Sequencing. Mol Cell. 2019;73(6):1292-1305.e8.
21. Stuart T, Butler A, Hoffman P, et al. Comprehensive Integration of Single-Cell Data. Cell. 2019;177(7):1888-1902.e21.
22. Korsunsky I, Millard N, Fan J, et al. Fast, sensitive and accurate integration of single-cell data with Harmony. Nat Methods. 2019;16(12):1289-1296.
23. Jin S, Guerrero-Juarez CF, Zhang L, et al. Inference and analysis of cell-cell communication using CellChat. Nat Commun. 2021;12(1):1088.
24. Kantarjian HM, Silver RT, Komrokji RS, Mesa RA, Tacke R, Harrison CN. Ruxolitinib for myelofibrosis--an update of its clinical effects. Clin Lymphoma Myeloma Leuk. 2013;13(6):638-645.

25. Wang H, He J, Xu C, et al. Decoding Human Megakaryocyte Development. Cell Stem Cell. 2021;28(3):535-549.e8.
26. Nakamura-Ishizu A, Matsumura T, Stumpf PS, et al. Thrombopoietin Metabolically Primes Hematopoietic Stem Cells to Megakaryocyte-Lineage Differentiation. Cell Rep. 2018;25(7):1772-1785.e6.
27. Hannigan G, Troussard AA, Dedhar S. Integrin-linked kinase: a cancer therapeutic target unique among its ILK. Nat Rev Cancer. 2005;5(1):51-63.
28. Strieter RM, Gomperts BN, Keane MP. The role of CXC chemokines in pulmonary fibrosis. J Clin Invest. 2007;117(3):549-556.
29. Przyklenk M, Georgieva VS, Metzen F, et al. LTBP1 promotes fibrillin incorporation into the extracellular matrix. Matrix Biol. 2022;110:60-75.
30. Liu Y, Huang A, Chen Q, et al. A distinct glycerophospholipid metabolism signature of acute graft versus host disease with predictive value. JCI Insight. 2019;5(16):e129494.
31. Yao JC, Oetjen KA, Wang T, et al. TGF-beta signaling in myeloproliferative neoplasms contributes to myelofibrosis without disrupting the hematopoietic niche. J Clin Invest. 2022;132(11):e154092.
32. Veglia F, Sanseviero E, Gabrilovich DI. Myeloid-derived suppressor cells in the era of increasing myeloid cell diversity. Nat Rev Immunol. 2021;21(8):485-498.
33. Li Z, Dong S, Huang S, et al. Role of CD34 in inflammatory bowel disease. Front Physiol. 2023;14:1144980.
34. Wu B, Rockel JS, Lagares D, Kapoor M. Ephrins and Eph Receptor Signaling in Tissue Repair and Fibrosis. Curr Rheumatol Rep. 2019;21(6):23.
35. Ubil E, Caskey L, Holtzhausen A, Hunter D, Story C, Earp HS. Tumor-secreted Pros1 inhibits macrophage M1 polarization to reduce antitumor immune response. J Clin Invest. 2018;128(6):2356-2369.
36. Omatsu M, Nakanishi Y, Iwane K, et al. THBS1-producing tumor-infiltrating monocyte-like cells contribute to immunosuppression and metastasis in colorectal cancer. Nat Commun. 2023;14(1):5534.
37. Stanietsky N, Simic H, Arapovic J, et al. The interaction of TIGIT with PVR and PVRL2 inhibits human NK cell cytotoxicity. Proc Natl Acad Sci U S A. 2009;106(42):17858-17863.
38. Solimando AG, Brandl A, Mattenheimer K, et al. JAM-A as a prognostic factor and new therapeutic target in multiple myeloma. Leukemia. 2018;32(3):736-743.

39. Zhou X, Liang S, Zhan Q, Yang L, Chi J, Wang L. HSPG2 overexpression independently predicts poor survival in patients with acute myeloid leukemia. Cell Death Dis. 2020;11(6):492.
40. Johnston RJ, Comps-Agrar L, Hackney J, et al. The immunoreceptor TIGIT regulates antitumor and antiviral CD8(+) T cell effector function. Cancer Cell. 2014;26(6):923-937.
41. Gangat N, Caramazza D, Vaidya R, et al. DIPSS plus: a refined Dynamic International Prognostic Scoring System for primary myelofibrosis that incorporates prognostic information from karyotype, platelet count, and transfusion status. J Clin Oncol. 2011;29(4):392-397.
42. Cervantes F, Pereira A, Esteve J, et al. Identification of 'short-lived' and 'long-lived' patients at presentation of idiopathic myelofibrosis. Br J Haematol. 1997;97(3):635-640.
43. Lopez-Novoa JM, Nieto MA. Inflammation and EMT: an alliance towards organ fibrosis and cancer progression. EMBO Mol Med. 2009;1(6-7):303-314.
44. Lecomte S, Devreux J, de Streel G, et al. Therapeutic activity of GARP:TGF-beta1 blockade in murine primary myelofibrosis. Blood. 2023;141(5):490-502.
45. Wang JC, Kundra A, Andrei M, et al. Myeloid-derived suppressor cells in patients with myeloproliferative neoplasm. Leuk Res. 2016;43:39-43.
46. Cimen Bozkus C, Roudko V, Finnigan JP, et al. Immune Checkpoint Blockade Enhances Shared Neoantigen-Induced T-cell Immunity Directed against Mutated Calreticulin in Myeloproliferative Neoplasms. Cancer Discov. 2019;9(9):1192-1207.
47. Harrison C, Kiladjian JJ, Al-Ali HK, et al. JAK inhibition with ruxolitinib versus best available therapy for myelofibrosis. N Engl J Med. 2012;366(9):787-798.
48. Mesa RA, Li CY, Schroeder G, Tefferi A. Clinical correlates of splenic histopathology and splenic karyotype in myelofibrosis with myeloid metaplasia. Blood. 2001;97(11):3665-3667.
49. Sonu R, Y Song J, Chen M. Extramedullary hematopoiesis associated with myeloproliferative neoplasm manifesting as pleural effusion: case report and review of literature. J Hematop. 2012;5(4):341-347.

Table 1. Clinicopathological features of the patients with primary myelofibrosis included in the study

Sample ID	Disease group	Age/ Sex	Grading of BM MF	Prior exposure	Driver mutation (VAF, %)*	Spleen size (cm)	PB blasts (%)	Hb (g/L)	Platelets (x 10^9/L)	WBC (x 10^9/L)	Neutrophil (x 10^9/L)	IPSS	DIPSS-Plus	MIPSS70 v2
MPN019	Pre-PMF	48/F	-	ANA	Triple negative	13.3	0	11.4	531	7,960	5,010	Int-1	Int-1	High
MPN038	Pre-PMF	55/F	-	HC	*CALR* (44.2)	11	0	12.5	799	6,540	3,530	Int-1	Int-1	Low
MPN052	Pre-PMF	56/M	-	HC	*JAK2* (1.1)	14	0	11.2	513	15,160	9,250	Int-2	Int-2	High
MPN099	Pre-PMF	62/M	-	No	*JAK2* (50.5)	15.9	0	12.9	788	17,230	12,580	Low	Low	Low
MPN111	Pre-PMF	76/F	-	No	*JAK2* (39.1)	11.6	0	13.9	1,256	20,240	15,990	Int-2	Int-2	Int
MPN015	Overt PMF	68/M	3	No	*JAK2* (22.6)	11.6	0	6.9	37	1,900	1,060	High	High	High
MPN016	Overt PMF	62/M	3	Off RUX	*CALR* (8.5)	26.8	7	6.1	294	33,590	18,140	High	High	High
MPN030	Overt PMF	38/F	2	HC, ANA	*CALR* (4.7)	10	0	9.5	761	11,910	8,580	Int-2	Int-2	Int
MPN035	Overt PMF	61/F	2	No	*JAK2* (74.3)	14.1	0	13.6	627	11,480	8,950	Low	Low	Low
MPN060	Overt PMF	53/M	3	Ongoing RUX	*CALR* (8.8)	>24	4	8.0	158	16,130	7,580	Int-1	Int-1	High
MPN063	Overt PMF	61/F	2	HC	*JAK2* (92.4)	18	0	10.6	246	15,940	12,910	Int-2	Int-1	Int
MPN068	Overt PMF	54/M	3	Ongoing RUX	*CALR* (5.3)	>23.5	5	8.2	69	6,210	3,290	Low	Low	Low
MPN071	Overt PMF	59/F	3	Ongoing RUX	*JAK2* (84.6)	24	6	8.2	211	8,710	4,700	Int-2	Int-2	High
MPN098	Overt PMF	61/M	3	No	*JAK2* (86.1)	30	1	10.9	287	12,300	7,380	Int-2	Int-2	Int
MPN101	Overt PMF	63/M	3	Off RUX, HC	*CALR* (8.5)	>21	10	7.4	203	34,760	17,030	High	High	High
MPN104	Overt PMF	53/M	3	No	Triple negative	13.8	1	5.1	21	1,100	180	High	Int-1	Int
MPN136	Overt PMF	53/M	3	Ongoing RUX	*CALR* (8.8)	>24	8	8.0	147	17,360	7,990	Int-1	Int-1	High

*All *CALR* mutations were type1, and the *JAK2* mutations were p.V617F. The VAF of the driver mutation was measured by NGS testing. NGS testing was performed on samples collected from six patients during treatment (MPN016, MPN060, MPN063, MPN071, MPN101, and MPN136), and remaining patients at the time of diagnosis.

PMF: primary myelofibrosis, F: female, M: male, ANA: agrylin, HC: hydrine, RUX: ruxolitinib, VAF: variant allele frequency, PB: peripheral blood, Hb: hemoglobin, WBC: white blood cell, IPSS: International Prognostic Scoring System, DIPSS: Dynamic International Prognostic Scoring System, MIPSS70: Mutation-enhanced International Prognostic Score System, Int: intermediate

Figure Legends

Figure 1. Single-cell profiling of bone marrow (BM) aspirates of patients with primary myelofibrosis (PMF) (A) The single-cell RNA sequencing data of BM aspirates from 17 patients with PMF were integrated. Two-dimensional uniform manifold approximation and projection (UMAP) visualization of 98,677 BM mononuclear cells identified 14 cell types after unsupervised clustering. Each point represents a single cell and is colored based on cell types. (B) UMAP plot colored by the clinical groups. (C) Cell type composition for each sample. Each box's color is consistent with the cell type. (D) Box plots representing the proportion of each cell type between pre-PMF (n = 5) and overt PMF (n = 12). The mean and 95% confidence interval are represented with black lines. pre-PMF, pre-fibrotic PMF; HSPC, hematopoietic stem and progenitor cell; MK, megakaryocyte, mDC, myeloid dendritic cell; pDC, plasmacytoid dendritic cell; NK, natural killer; PC, plasma cell; MSC, mesenchymal stromal cell.

Figure 2. Hematopoietic stem and progenitor cell (HSPC) subsets and their gene signatures (A) Uniform manifold approximation and projection (UMAP) plot colored by HSPC subsets. (B) Box plots representing the proportion of each HSPC subset. The mean and 95% confidence interval are represented with black lines. (C) Megakaryocyte (MK) signature scores are shown in the UMAP plot by the clinical groups (upper panels) and the violin plot by HSPC subsets (lower panels). (D) The expression levels of *MPIG6B* and *PF4* are shown by clinical groups. PMF, primary myelofibrosis; pre-PMF, pre-fibrotic PMF; HSC, hematopoietic stem cell; MEMP, megakaryocyte-erythroid-mast progenitor; MEP, megakaryocyte-erythroid progenitor; GMP, granulocyte-monocyte progenitor.

Figure 3. Megakaryocyte (MK) subsets and their gene signatures (A) Uniform manifold approximation and projection (UMAP) plot colored by MK subsets. (B) Box plots representing the proportion of each MK subset. The mean and 95% confidence interval are represented with black lines. (C) Signature scores are shown in the violin plot by MK subsets. (D) The heatmap shows the 19 differentially expressed genes in MK between pre-PMF and overt PMF. Red and blue colors indicate up-regulated and down-regulated genes, respectively. PMF, primary myelofibrosis; pre-PMF, pre-fibrotic PMF.

Figure 4. T and natural killer (NK) subsets (A) Uniform manifold approximation and projection (UMAP) plot colored by T and NK subsets. (B) Dot plot of subset-specific marker genes per T or NK subset. Dot intensity (from blue to red) represents the average expression value of all cells per T or NK subset, whereas dot size represents the proportion of cells expressing the genes. (C) The expression level of cytotoxic signature score is shown in the violin plot by T and NK subsets. (D) Box plots represent the proportion of dysfunctional gene-expressing cytotoxic terminal effector cells by the clinical groups. The mean and 95% confidence interval are represented with black lines. PMF, primary myelofibrosis; pre-PMF, pre-fibrotic PMF; Treg, regulatory T; MAIT, mucosal-associated invariant T; Tmem, cytotoxic memory; Teff, cytotoxic terminal effector.

Figure 5. $CD14^+$ monocyte subsets (A) Uniform manifold approximation and projection (UMAP) plot colored by $CD14^+$ monocyte subsets. (B) Dot plot of subset-specific marker genes per monocyte subset. Dot intensity (from blue to red) represents the average expression value of all cells per monocyte subset, whereas dot size represents the proportion of cells expressing the genes. Monocytic myeloid-derived suppressor cell (M-MDSC) markers are highlighted in a red box. (C) Box plots represent the proportion of Mono3 (M-MDSC) subset

by the clinical groups. The mean and 95% confidence interval are represented with black lines. (D) The expression level of the interferon signature score is shown in the violin plot by monocyte subsets. PMF, primary myelofibrosis; pre-PMF, pre-fibrotic PMF.

Figure 6. Cell–cell communication analyses A bar plot represents signaling pathways, ranked according to the differences in overall information flow within the inferred networks between pre-PMF and overt PMF. The overall information flow of a signaling network is calculated by summarizing all the communication probabilities within the network. Signaling pathways that are more enriched in overt PMF are marked in pink, whereas those more enriched in pre-PMF are marked in blue. PMF, primary myelofibrosis; pre-PMF, pre-fibrotic PMF.

Figure 7. Representative interaction pathways (A-B) Circle plots represent the inferred interaction pathways of (A) CD34 and CD40, which were exclusively identified in overt PMF, and those of (B) TGF-β, identified in both pre-PMF and overt PMF. Edge width represents the communication probability (strength of the interactions) between cell populations. Edge colors are consistent with the signaling source. (C) The expression of ligands and receptors for EPHB, CD34, CD40, TGF-β, and TIGIT in each cell subset from pre-PMF (blue) and overt PMF (red) is shown. Genes corresponding to ligands in each signaling pathway are indicated in bold. Major sources and targets of each signaling pathway are highlighted with boxes. MK5 from pre-PMF was excluded owing to a low number of cells. Details are described in the Supplemental Methods. PMF, primary myelofibrosis; pre-PMF, pre-fibrotic PMF; HSC, hematopoietic stem cell; MEMP, megakaryocyte-erythroid-mast progenitor; MEP, megakaryocyte-erythroid progenitor; GMP, granulocyte-monocyte progenitor; MK, megakaryocyte; Treg, regulatory T; MAIT, mucosal-associated invariant T; Tmem, cytotoxic

memory; Teff, cytotoxic terminal effector; NK, natural killer; $CD56^{bright}$, $CD56^{bright}$ NK; $CD14^{+}$, $CD14^{+}$ monocyte; M-MDSC, monocytic myeloid-derived suppressor cell; $CD16^{+}$, $CD16^{+}$ monocyte; ERY, erythroid; PC, plasma cell; mDC, myeloid dendritic cell; NP, Neutrophil; MSC, mesenchymal stromal cell.

Figure 1

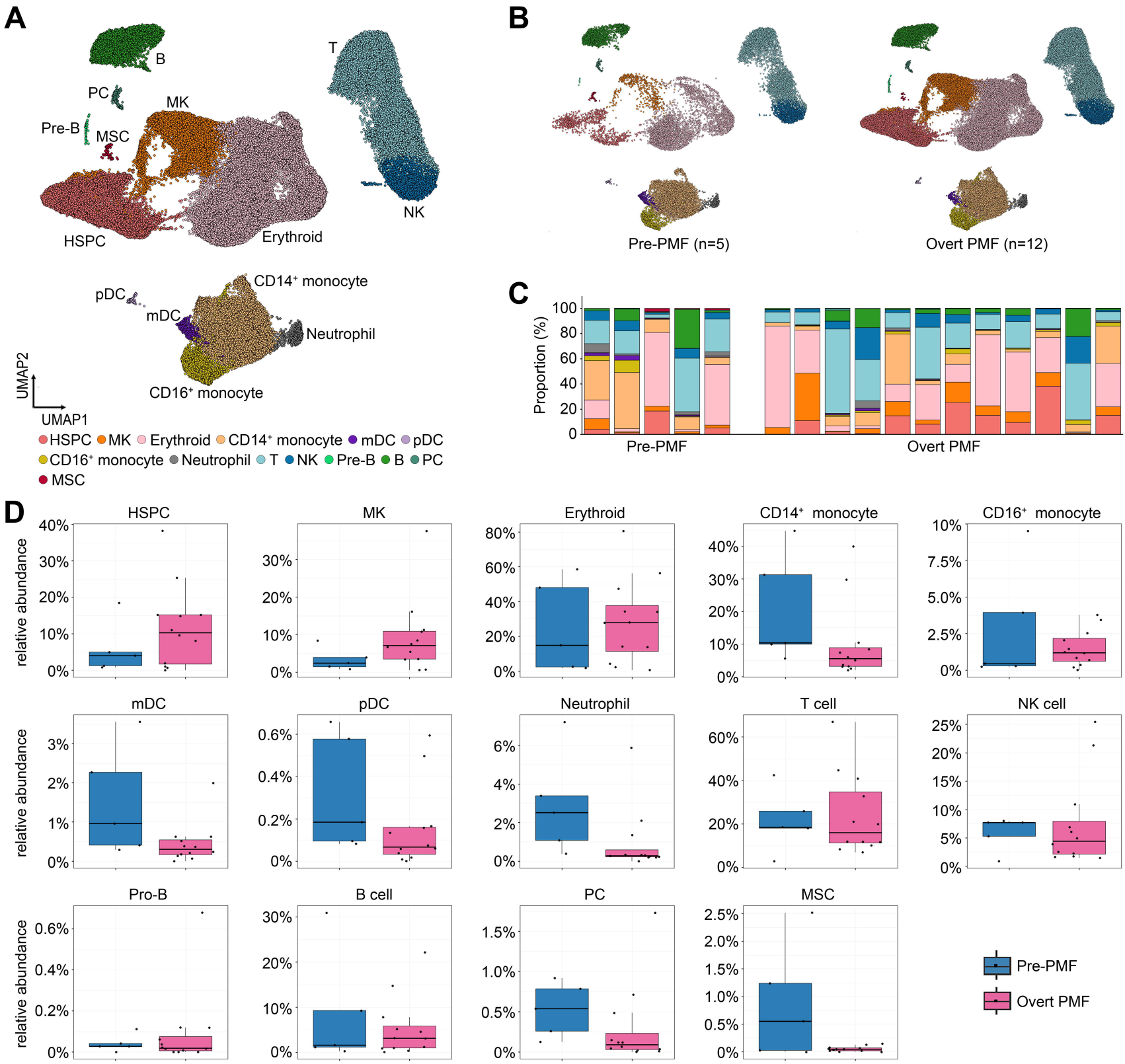
A
B
T
PC
MK
Pre-B
MSC
NK
HSPC
Erythroid
pDC
CD14⁺ monocyte
mDC
Neutrophil
CD16⁺ monocyte
UMAP2
UMAP1
HSPC MK Erythroid CD14⁺ monocyte mDC pDC
CD16⁺ monocyte Neutrophil T NK Pre-B B PC
MSC
B
Pre-PMF (n=5)
Overt PMF (n=12)
C
Proportion (%)
100
80
60
40
20
0
Pre-PMF
Overt PMF
D
HSPC
MK
Erythroid
CD14⁺ monocyte
CD16⁺ monocyte
mDC
pDC
Neutrophil
T cell
NK cell
Pro-B
B cell
PC
MSC
relative abundance
Pre-PMF
Overt PMF

Figure 2

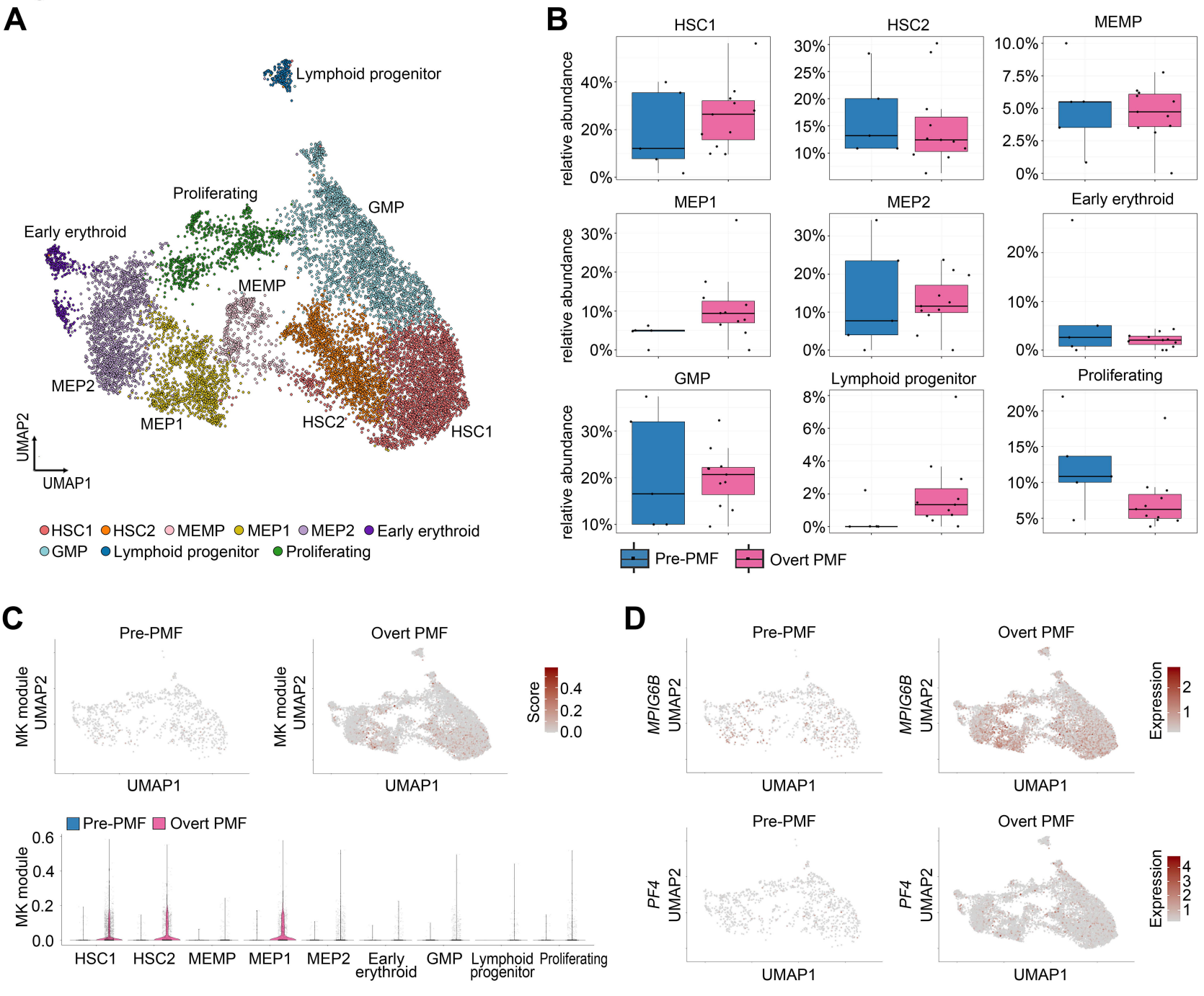
A
Lymphoid progenitor
Proliferating
GMP
Early erythroid
MEMP
MEP2
MEP1
HSC2
HSC1
UMAP2
UMAP1
HSC1 HSC2 MEMP MEP1 MEP2 Early erythroid
GMP Lymphoid progenitor Proliferating
B
HSC1
HSC2
MEMP
MEP1
MEP2
Early erythroid
GMP
Lymphoid progenitor
Proliferating
relative abundance
Pre-PMF
Overt PMF
C
Pre-PMF
Overt PMF
MK module UMAP2
UMAP1
Score
MK module
Pre-PMF Overt PMF
HSC1 HSC2 MEMP MEP1 MEP2 Early erythroid GMP Lymphoid progenitor Proliferating
D
Pre-PMF
Overt PMF
MPIG6B UMAP2
PF4 UMAP2
UMAP1
Expression

Figure 3

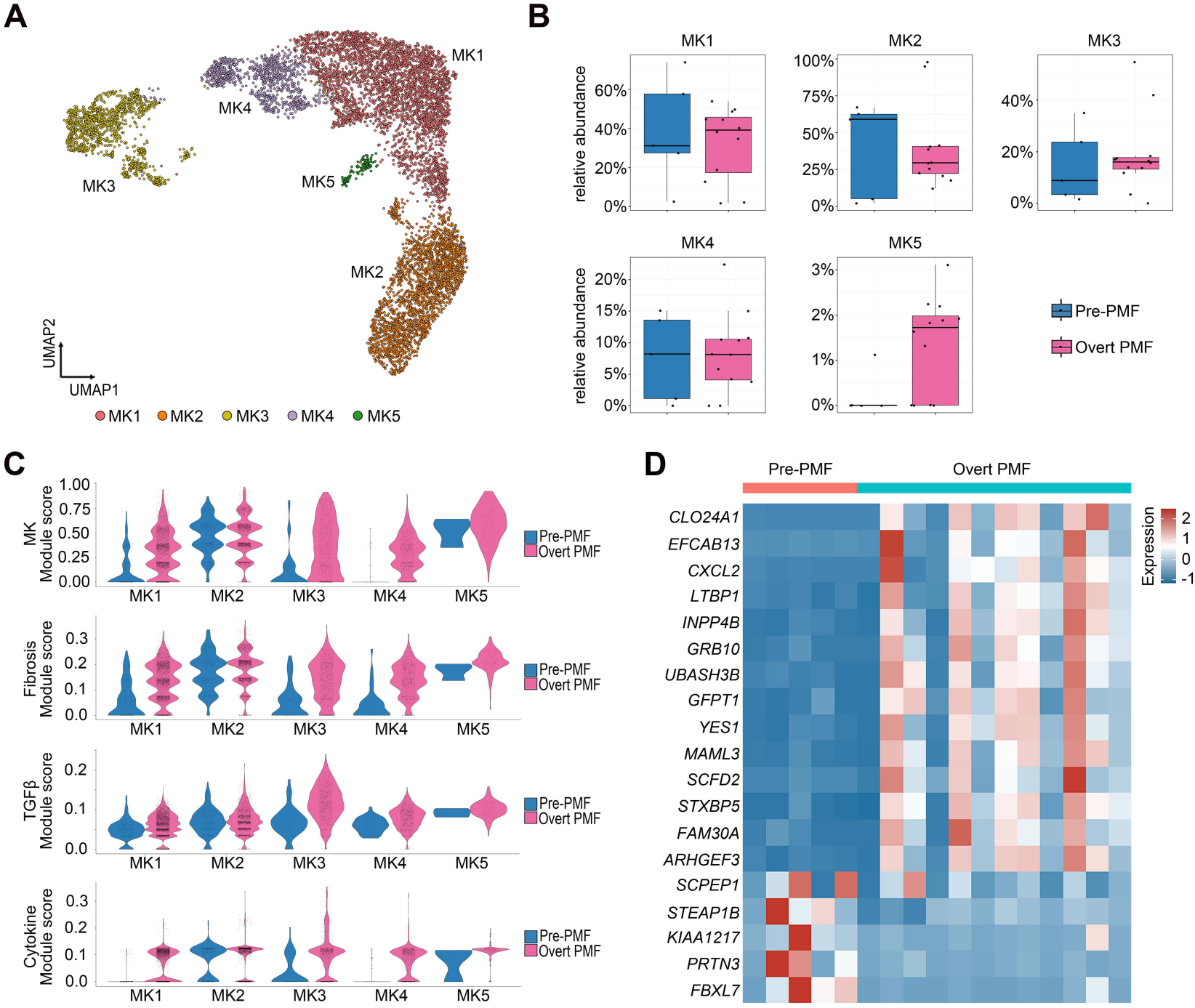
A
MK1
MK2
MK3
MK4
MK5
UMAP1
UMAP2
B
relative abundance
Pre-PMF
Overt PMF
C
MK Module score
Fibrosis Module score
TGFβ Module score
Cytokine Module score
D
Pre-PMF
Overt PMF
CLO24A1
EFCAB13
CXCL2
LTBP1
INPP4B
GRB10
UBASH3B
GFPT1
YES1
MAML3
SCFD2
STXBP5
FAM30A
ARHGEF3
SCPEP1
STEAP1B
KIAA1217
PRTN3
FBXL7
Expression

Figure 4

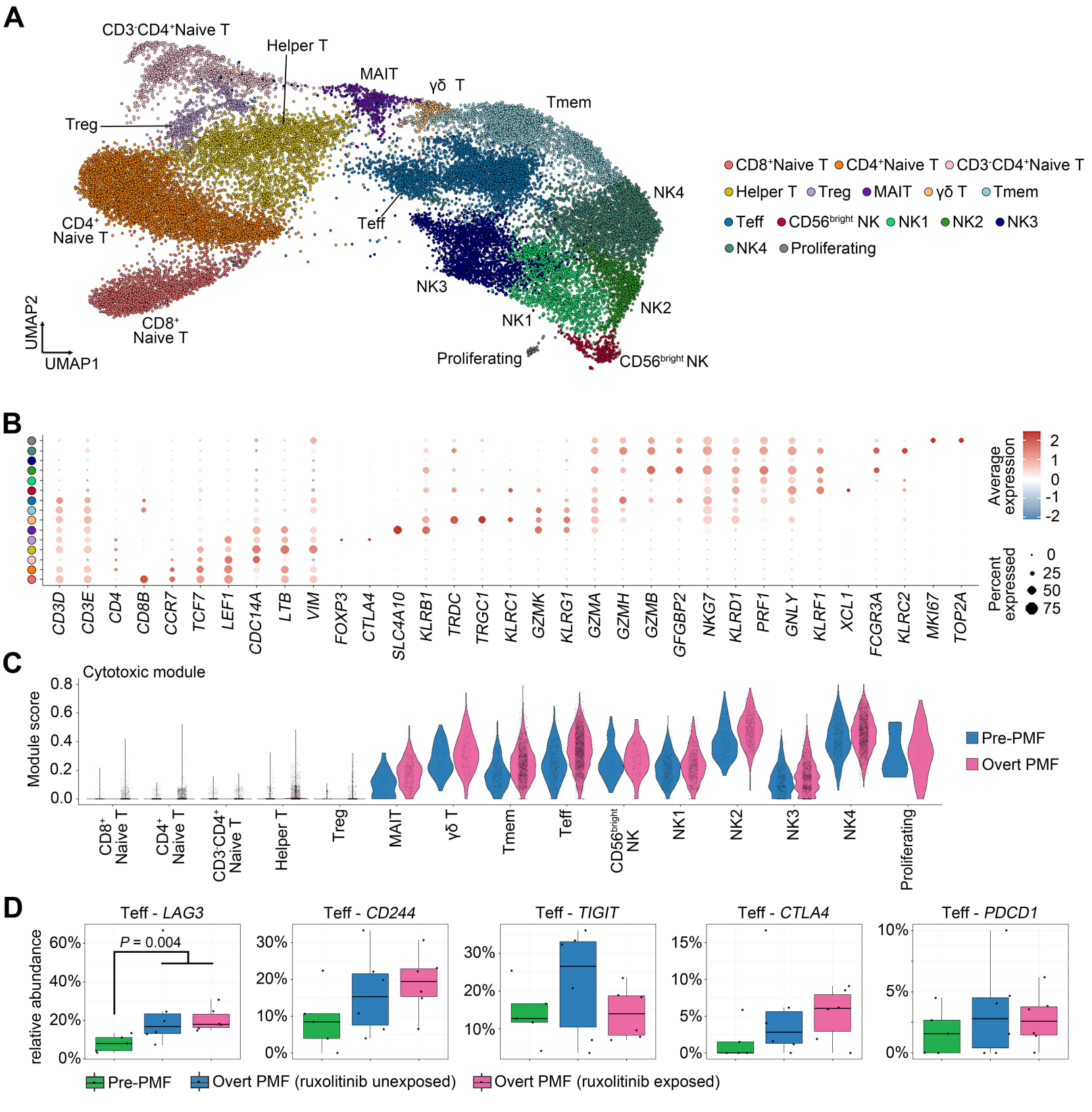
A
CD3-CD4+Naive T
Helper T
MAIT
γδ T
Tmem
Treg
CD4+ Naive T
Teff
NK4
NK3
NK2
NK1
CD8+ Naive T
Proliferating
CD56bright NK
UMAP2
UMAP1
CD8+Naive T
CD4+Naive T
CD3-CD4+Naive T
Helper T
Treg
MAIT
γδ T
Tmem
Teff
CD56bright NK
NK1
NK2
NK3
NK4
Proliferating
B
CD3D
CD3E
CD4
CD8B
CCR7
TCF7
LEF1
CDC14A
LTB
VIM
FOXP3
CTLA4
SLC4A10
KLRB1
TRDC
TRGC1
KLRC1
GZMK
KLRG1
GZMA
GZMH
GZMB
GFGBP2
NKG7
KLRD1
PRF1
GNLY
KLRF1
XCL1
FCGR3A
KLRC2
MKI67
TOP2A
Average expression
2
1
0
-1
-2
Percent expressed
0
25
50
75
C
Cytotoxic module
Module score
0.8
0.6
0.4
0.2
0.0
CD8+ Naive T
CD4+ Naive T
CD3-CD4+ Naive T
Helper T
Treg
MAIT
γδ T
Tmem
Teff
CD56bright NK
NK1
NK2
NK3
NK4
Proliferating
Pre-PMF
Overt PMF
D
Teff - LAG3
Teff - CD244
Teff - TIGIT
Teff - CTLA4
Teff - PDCD1
relative abundance
P = 0.004
60%
40%
20%
0%
30%
20%
10%
0%
30%
20%
10%
15%
10%
5%
0%
10%
5%
0%
Pre-PMF
Overt PMF (ruxolitinib unexposed)
Overt PMF (ruxolitinib exposed)

Figure 5

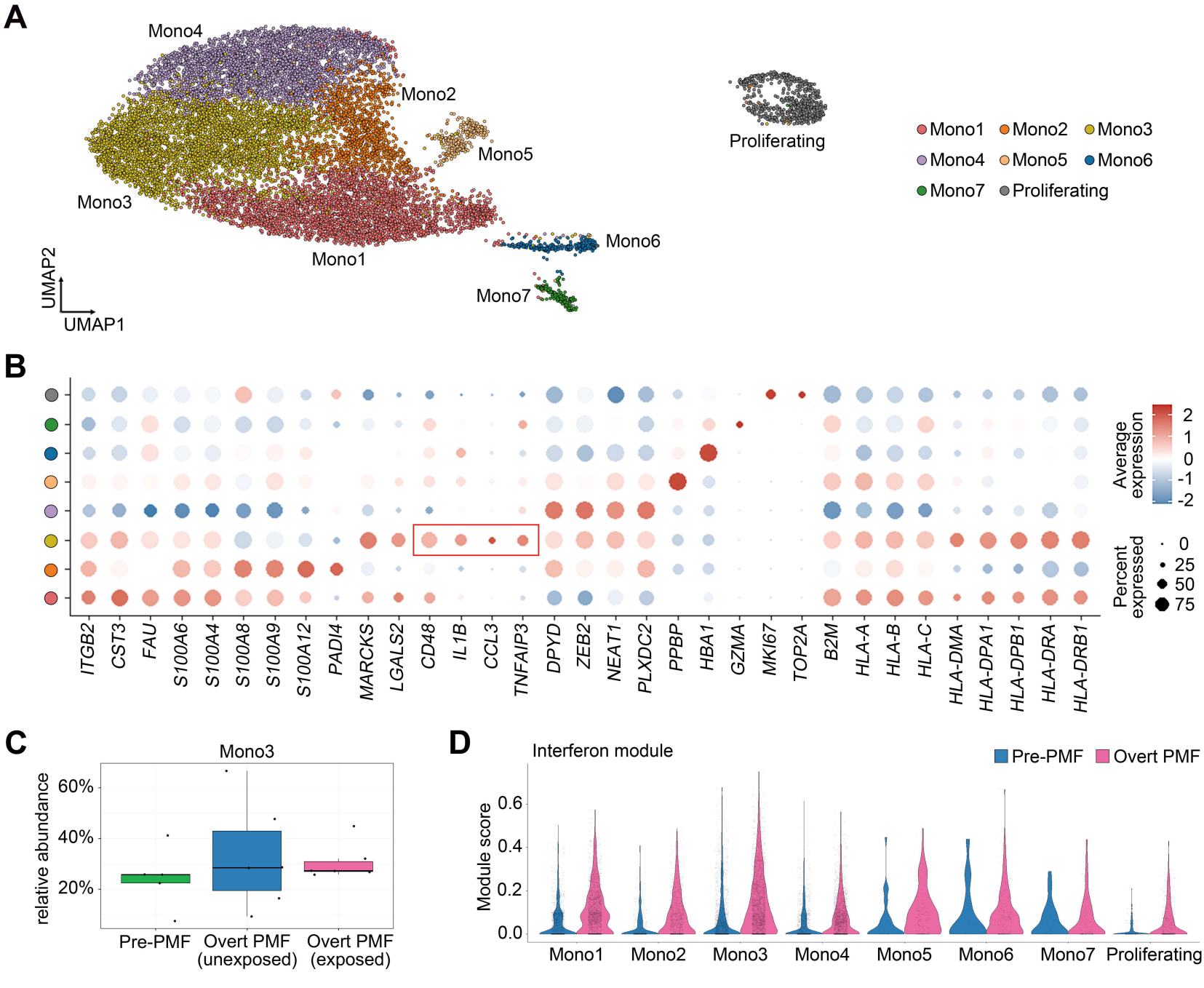
A
Mono4
Mono2
Mono5
Mono3
Mono1
Mono6
Mono7
Proliferating
Mono1 Mono2 Mono3
Mono4 Mono5 Mono6
Mono7 Proliferating
UMAP2
UMAP1
B
Average expression
2
1
0
-1
-2
Percent expressed
0
25
50
75
ITGB2 CST3 FAU S100A6 S100A4 S100A8 S100A9 S100A12 PADI4 MARCKS LGALS2 CD48 IL1B CCL3 TNFAIP3 DPYD ZEB2 NEAT1 PLXDC2 PPBP HBA1 GZMA MKI67 TOP2A B2M HLA-A HLA-B HLA-C HLA-DMA HLA-DPA1 HLA-DPB1 HLA-DRA HLA-DRB1
C
Mono3
relative abundance
60%
40%
20%
Pre-PMF
Overt PMF (unexposed)
Overt PMF (exposed)
D
Interferon module
Pre-PMF
Overt PMF
Module score
0.6
0.4
0.2
0.0
Mono1 Mono2 Mono3 Mono4 Mono5 Mono6 Mono7 Proliferating

Figure 6

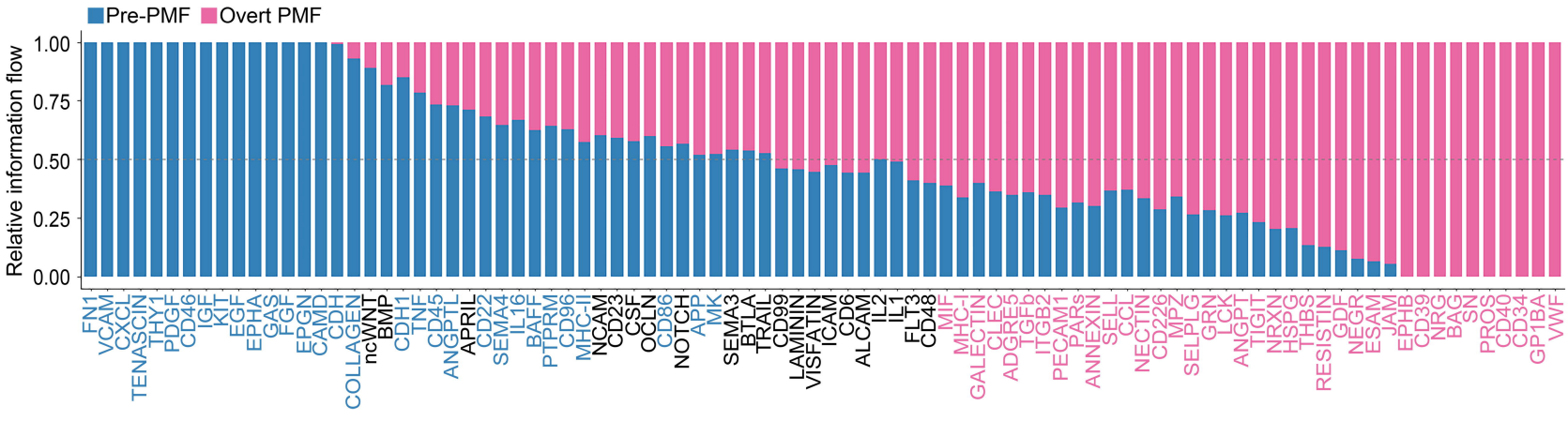
Pre-PMF
Overt PMF
Relative information flow
1.00
0.75
0.50
0.25
0.00
FN1
VCAM
CXCL
TENASCIN
THY1
PDGF
CD46
IGF
KIT
EGF
EPHA
GAS
FGF
EPGN
CAMD
CDH
COLLAGEN
ncWNT
BMP
CDH1
TNF
CD45
ANGPTL
APRIL
CD22
SEMA4
IL16
BAFF
PTPRM
CD96
MHC-II
NCAM
CD23
CSF
OCLN
CD86
NOTCH
APP
MK
SEMA3
BTLA
TRAIL
CD99
LAMININ
VISFATIN
ICAM
CD6
ALCAM
IL2
IL1
FLT3
CD48
MIF
MHC-I
GALECTIN
CLEC
ADGRE5
TGFb
ITGB2
PECAM1
PARs
ANNEXIN
SELL
CCL
NECTIN
CD226
MPZ
SELPLG
GRN
LCK
ANGPT
TIGIT
NRXN
HSPG
THBS
RESISTIN
GDF
NEGR
ESAM
JAM
EPHB
CD39
NRG
BAG
SN
PROS
CD40
CD34
GP1BA
VWF

Figure 7

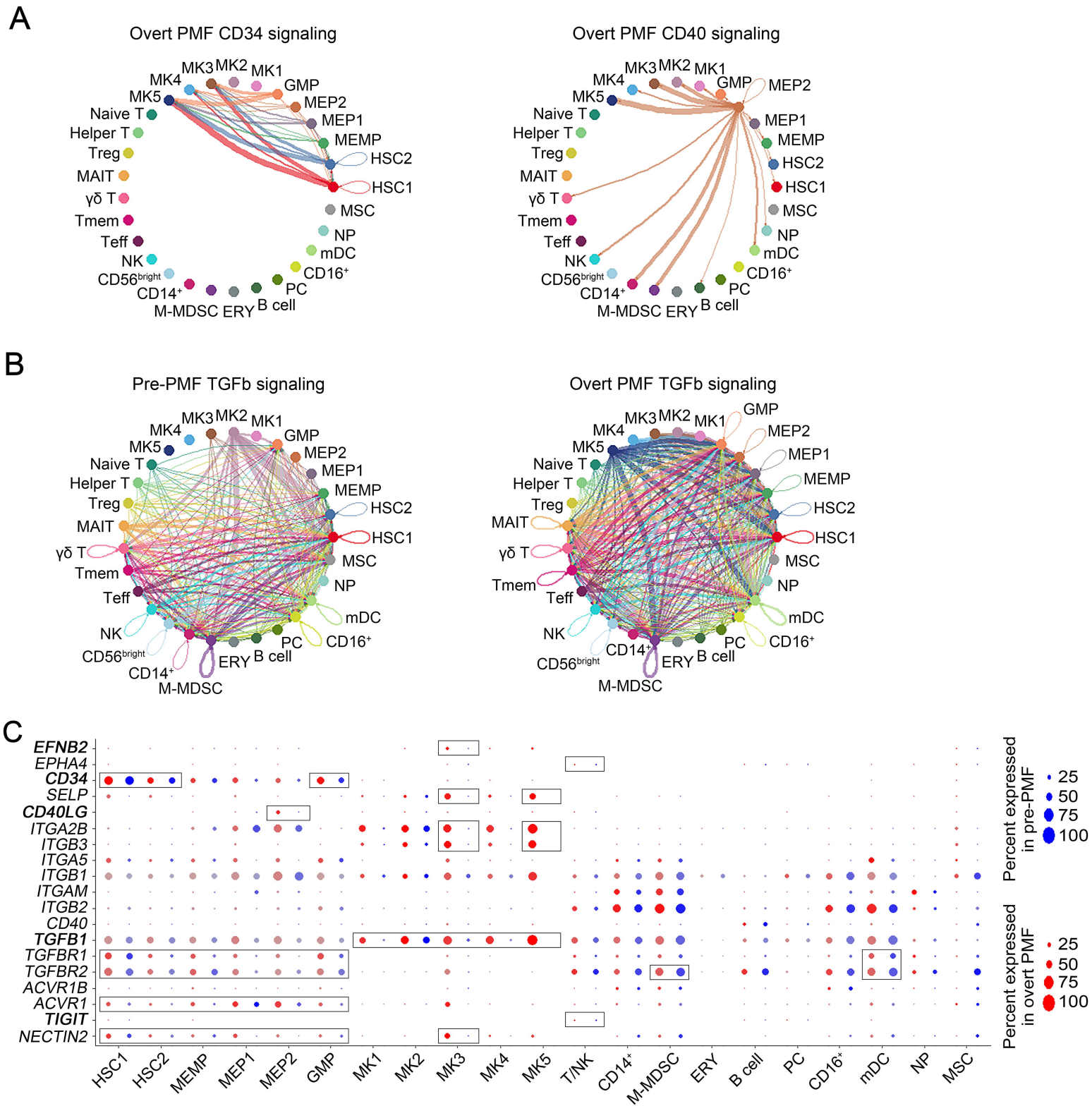
A
Overt PMF CD34 signaling
Overt PMF CD40 signaling
B
Pre-PMF TGFb signaling
Overt PMF TGFb signaling
C
EFNB2
EPHA4
CD34
SELP
CD40LG
ITGA2B
ITGB3
ITGA5
ITGB1
ITGAM
ITGB2
CD40
TGFB1
TGFBR1
TGFBR2
ACVR1B
ACVR1
TIGIT
NECTIN2
HSC1 HSC2 MEMP MEP1 MEP2 GMP MK1 MK2 MK3 MK4 MK5 T/NK CD14+ M-MDSC ERY B cell PC CD16+ mDC NP MSC
Percent expressed in pre-PMF
25
50
75
100
Percent expressed in overt PMF
25
50
75
100

Supplementary Materials

Table of Contents

Supplementary Methods……...page 2

Supplementary Figure 1……page 5

Supplementary Figure 2……page 7

Supplementary Figure 3……page 8

Supplementary Figure 4……page 9

Supplementary Figure 5……page 10

Supplementary Figure 6……..…….page 11

Supplementary Figure 7……..…….page 13

Supplementary Table 1……..……...page 14

Supplementary Table 2……..……...page 15

Supplementary References……...page 16

Supplemental Methods

Bone marrow samples

The PMF diagnosis was made with BM biopsies based on the 2016 WHO criteria and involved a composite assessment of clinical and laboratory features.[1] The diagnosis of post-ET-MF and post-PV-MF adheres to the criteria published by the International Working Group for MPN Research and Treatment.[2] For scRNA-seq, we used BM aspirates from 33 patients with MPN. The 33 patients consisted of five ETs, one PV, 17 PMF (five pre-PMFs and 12 overt PMFs), and ten post-MF (six post-ET-MFs and four post-PV-MFs). Among the 12 patients with overt PMF, six were treated with the JAK inhibitor ruxolitinib, while the remaining six were not treated with any JAK inhibitor. To minimize the risk of PB dilution in BM aspirate samples, we repeated the aspiration at a different site if a dry tap was encountered during the procedure. We also performed microscopic examination of the BM aspirates to assess their quality and composition. The patients' BM fibrosis was confirmed by the BM biopsy, indicating that our aspirates represented remaining fluidic areas that the fibrotic PMF-BM surrounded. We obtained 16 mL (8 mL x 2 bottles) of BM aspirates from each patient. The mean of mononuclear cell yield for the MF patient aspirates was 1.1×10^8 cells (range, $1.9 \times 10^7 – 2.5 \times 10^8$). This study was approved by the institutional review board of the Catholic University of Korea, College of Medicine (KC20TISI0206). All specimens from the patients in this study were obtained with appropriate consent in accordance with the declaration of Helsinki.

BM aspirates were filtered through a 100 μm Cell Strainer (SPL Life Sciences), then layered onto a Ficolle-Paque PLUS (GE Healthcare) gradient. The sample was centrifuged at 2,500 rpm for 30 min. The isolated mononuclear cells were subsequently washed with Phosphate Buffered Saline (HyClone). After removing red blood cells using RBC lysis buffer (Miltenyi Biotec), the cells were counted and cryopreserved in freezing medium (10% DMSO + 90% FBS) at −80 °C until use.

scRNA-seq library construction

Chromium Single Cell 3' v3 Reagent kit (10x Genomics, Pleasanton, CA, USA) was used for the library construction of scRNA-seq according to the manufacturer's protocol. In brief, single-cell suspension was counted by hemocytometer (Thermo Fisher Scientific, Waltham, MA) and loaded into a Chromium instrument system targeting 10,000 cells. The cells were then partitioned into gel beads in emulsion in the Chromium instrument (10x Genomics), where cell lysis and barcoded reverse transcription of RNA occurred. Complementary DNA (cDNA) was synthesized and amplified for 14 cycles. cDNA clean-up was performed using a SPRIselect Reagent Kit (Beckman Coulter, Brea, CA). 50 ng of the amplified cDNA was used for each sample to construct indexed sequencing libraries. Sequencing libraries were sequenced on the Illumina NovaSeq platform (Illumina, San Diego, CA). Raw sequencing data generated for scRNA-sequencing have been deposited in Sequence Read Archive under accession number PRJNA1070224.

scRNA-seq data analysis

The sequenced data were processed into the expression matrices with the CellRanger 3.1.0 (10x Genomics). Sequencing reads were mapped to the GRCh38 reference genome, followed by unique molecular identifier (UMI) and barcode counting, and the UMI count matrices were constructed. Bioinformatics processing of the scRNA-sequencing data was performed with the R package Seurat.[3] To exclude low-quality cells in scRNA-sequencing, we filtered cells with an expressed gene count of fewer than 200 or cells with more than 20% of reads corresponding to mitochondrial genes. Additionally, doublets were excluded using Scrublet.[4] Data was log-normalized, and highly variable features were identified based on a variance stabilizing transformation method. All individual datasets were then integrated using the Harmony

algorithm.[5] Principal components analysis and graph-based clustering were performed on the integrated datasets, and the clustering data were then applied to the uniform manifold approximation and projection. Each cell cluster was annotated for its cell type using the SingleR[6] and the well-known cell-type-specific markers.

Cell cycle analysis was performed by using the 'CellCycleScoring' function in Seurat. Differentially expressed gene (DEG) analysis was used to identify significant DEGs within each cluster using the 'FindMarkers' function in Seurat. We kept only genes with an average $\log_2$ fold-change value greater than 1 and an adjusted *P* value (false discovery rate) lower than 0.2 in the analysis. Gene signature scores were calculated based on the Mann-Whitney U statistic using UCell.[7] Gene set enrichment analysis was performed using fgsea with the 'HALLMARK' gene set downloaded from MSigDB.[8] To compare MK subset abundance between PMF and other MPN diseases, MK cells of 16 MPN patients (five ET, one PV, six post-ET-MF, and four post-PV-MF) were projected onto the MK subsets of PMF patients using the "TransferData" function in Seurat.

To examine the cell-to-cell communication between different cell subsets in the PMF-BM, receptor-ligand (LR) interactions were analyzed using CellChat.[9] The LR pairs in CellChat retrieved from the previous studies were divided into four groups: cytokine/chemokine, immune checkpoint, growth factor, and others.[9] Four rare cell populations (pDC, pre-B, and two HSPC subsets [early erythroid and lymphoid progenitor]) were excluded from the analysis. To simplify the data, some cell subsets were merged as follows; naïve T ($CD8^+$Naïve T, $CD4^+$Naïve T, and $CD3^-CD4^+$Naïve T), NK (NK1, NK2, NK3, and NK4), and monocyte (mono1, mono2, mono4, mono5, mono6, and mono7). To compare the CellChat results between normal BM and MM BM, the 'liftCellChat' function was used. Cell-cell communications, if there are only a few cells (< 10) in certain cell groups, were filtered out.

Supplementary Figures

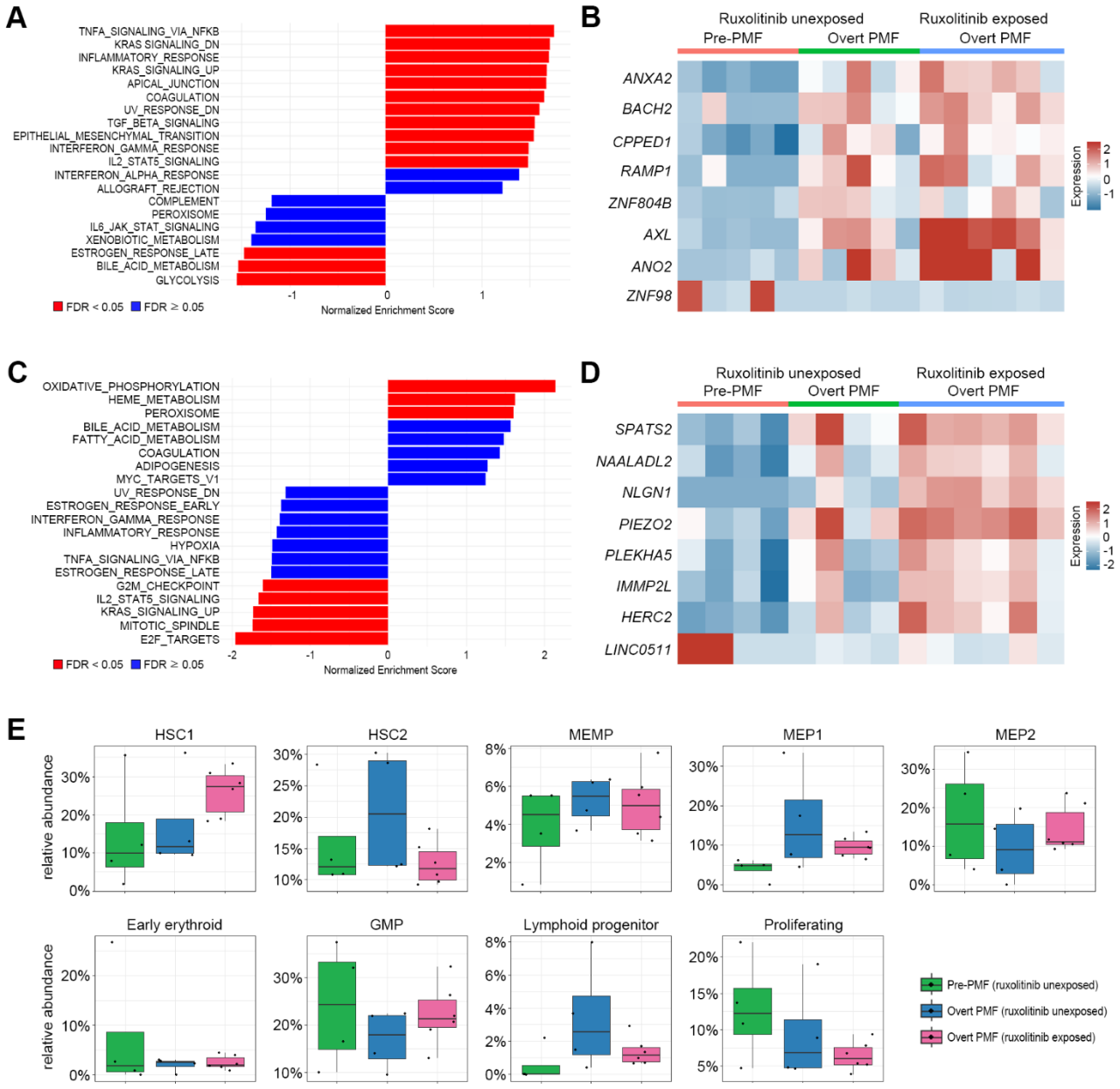

Supplementary Fig. 1. HSPC subsets and gene signatures. (A) The top 20 statistically-enriched 'HALLMARK' gene sets for the HSC1 subset. The x-axis represents the normalized enrichment score. (B) The heatmap shows the eight DEGs in the HSC1 subset between pre-PMF and overt PMF (seven up-regulated and one down-regulated in overt PMF). Red and blue colors indicate up-regulated and down-regulated genes, respectively. (C) The top 20 statistically enriched 'HALLMARK' gene sets for MEP1 subset. GSEA analysis revealed enrichment in the MK-lineage differentiation,[10-12] including 'oxidative phosphorylation', 'peroxisome', and 'coagulation'. The x-axis represents the normalized enrichment score. (D) The heatmap shows the eight DEGs in the MEP1 subset between pre-PMF and

overt-PMF (seven up-regulated and one down-regulated in overt PMFs). Red and blue colors indicate up-regulated and down-regulated genes, respectively. (E) Box plots representing the proportion of each cell type between pre-PMF (n = 5), ruxolitinib-unexposed overt PMF (n=6), and ruxolitinib-exposed overt PMF (n = 6). The mean and 95% confidence interval are represented with black lines.

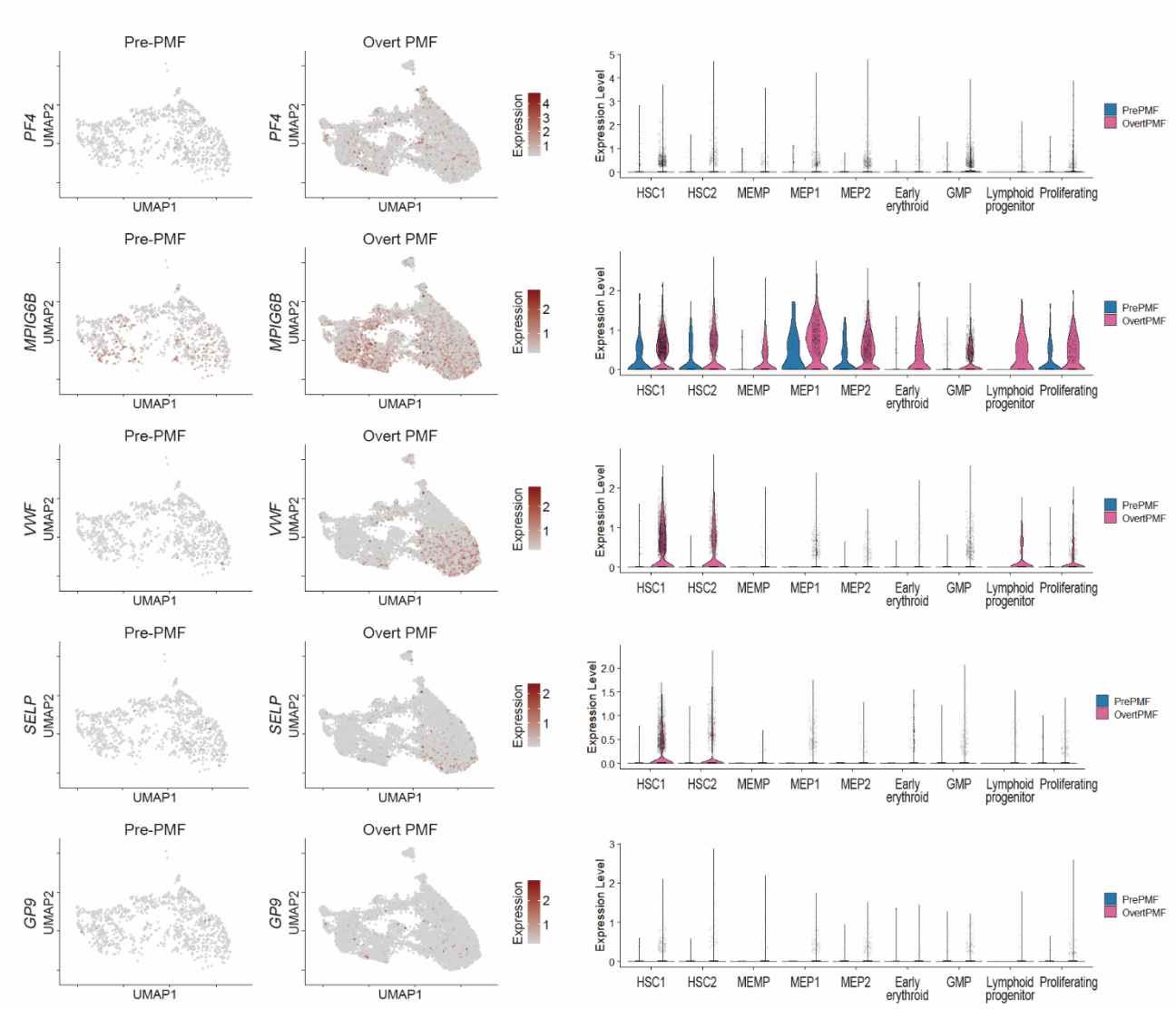

Supplementary Fig. 2. HSPC subsets and their MK signature genes. The expression level of MK signature genes is shown in the UMAP plot by the clinical groups (left panels) and the violin plot by HSPC subsets (right panels).

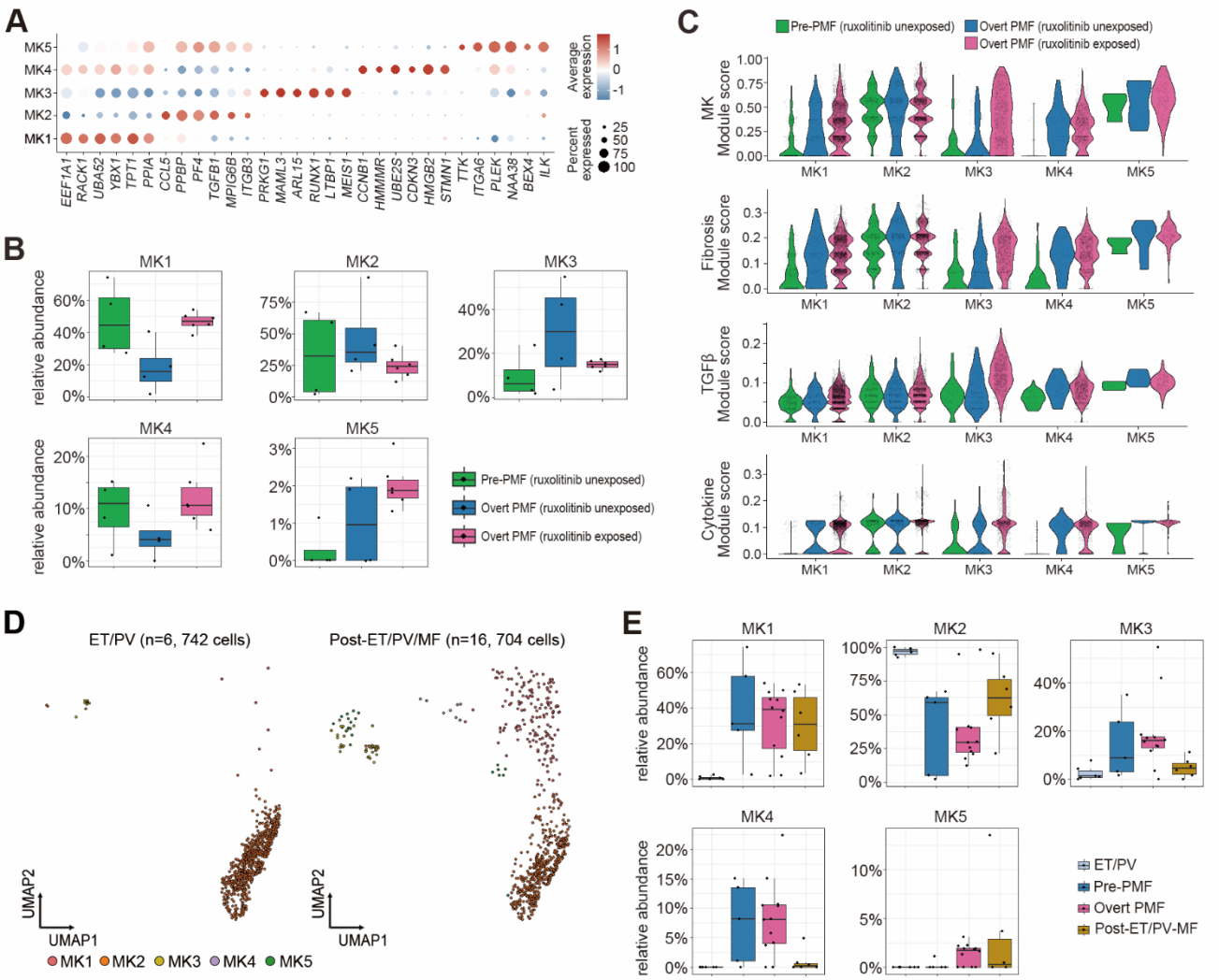

Supplementary Fig. 3. MK subsets and their gene signatures. (A) Dot plot of subset-specific marker genes per MK subset. Dot intensity (from blue to red) represents the average expression value of all cells per MK subset, whereas dot size represents the proportion of cells expressing the genes. (B) Box plots represent the proportion of each MK subset between pre-PMF (n = 5), ruxolitinib unexposed overt PMF (n=6), and ruxolitinib exposed overt PMF (n = 6). The mean and 95% confidence interval are represented with black lines. (C) Signature scores are shown in the violin plot by MK subsets. (D) MK subsets in non-PMF MPNs. UMAP plot colored by MK subsets. (E) Box plots represent the proportion of each MK subset between ET/PV (n = 6), pre-PMF (n = 5), overt PMF (n = 12), and post-ET/PV-MF (n = 10). The mean and 95% confidence interval are represented with black lines. The overt-PMF-specific MK5 subset was observed in post-ET/PV-MF patients (three out of six patients with more than 10 MK cells), but not in ET/PV.

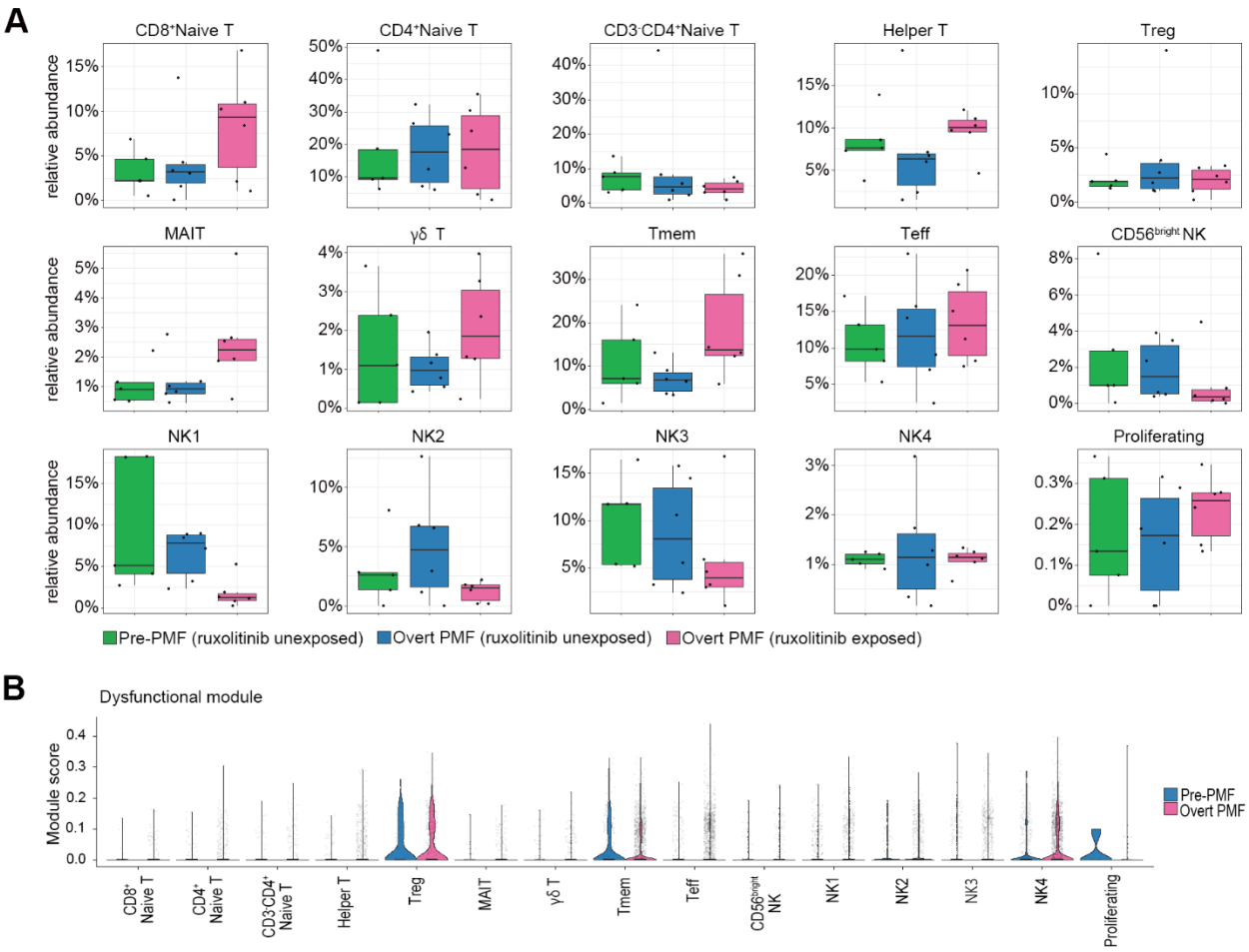

Supplementary Fig. 4. The subset abundance and dysfunctional module score of T and NK cell populations. (A) Box plots represent the proportion of each T and NK subset between pre-PMF (n = 5), ruxolitinib unexposed overt PMF (n=6), and ruxolitinib exposed overt PMF (n = 6). The mean and 95% confidence interval are represented with black lines. (B) The expression level of dysfunctional signature score is shown in the violin plot by T and NK subsets.

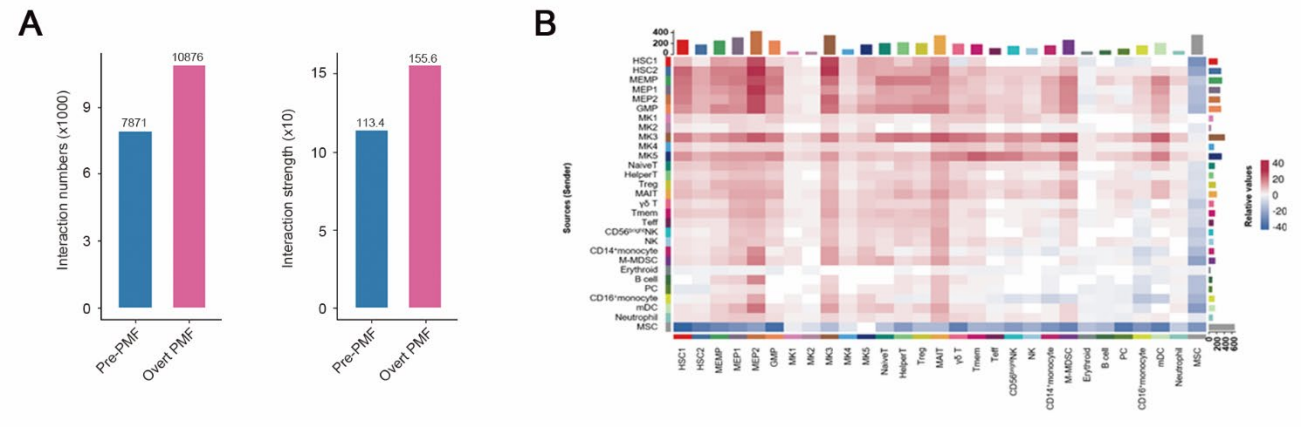

Supplementary Fig. 5. Visualization of cell-cell communication. (A) Comparison of the total number of interactions and strength of these interactions between pre-PMF and overt PMF. (B) Differential number of ligand-receptor (LR) interactions between pre-PMF and overt PMF. The total number of enriched LR interactions is shown as a bar on the x-axis and y-axis, and the relative strength of the interactions (pre-PMF vs overt PMF) is shown in the heatmap. Red and blue indicate enrichment of overt PMF and pre-PMF, respectively.

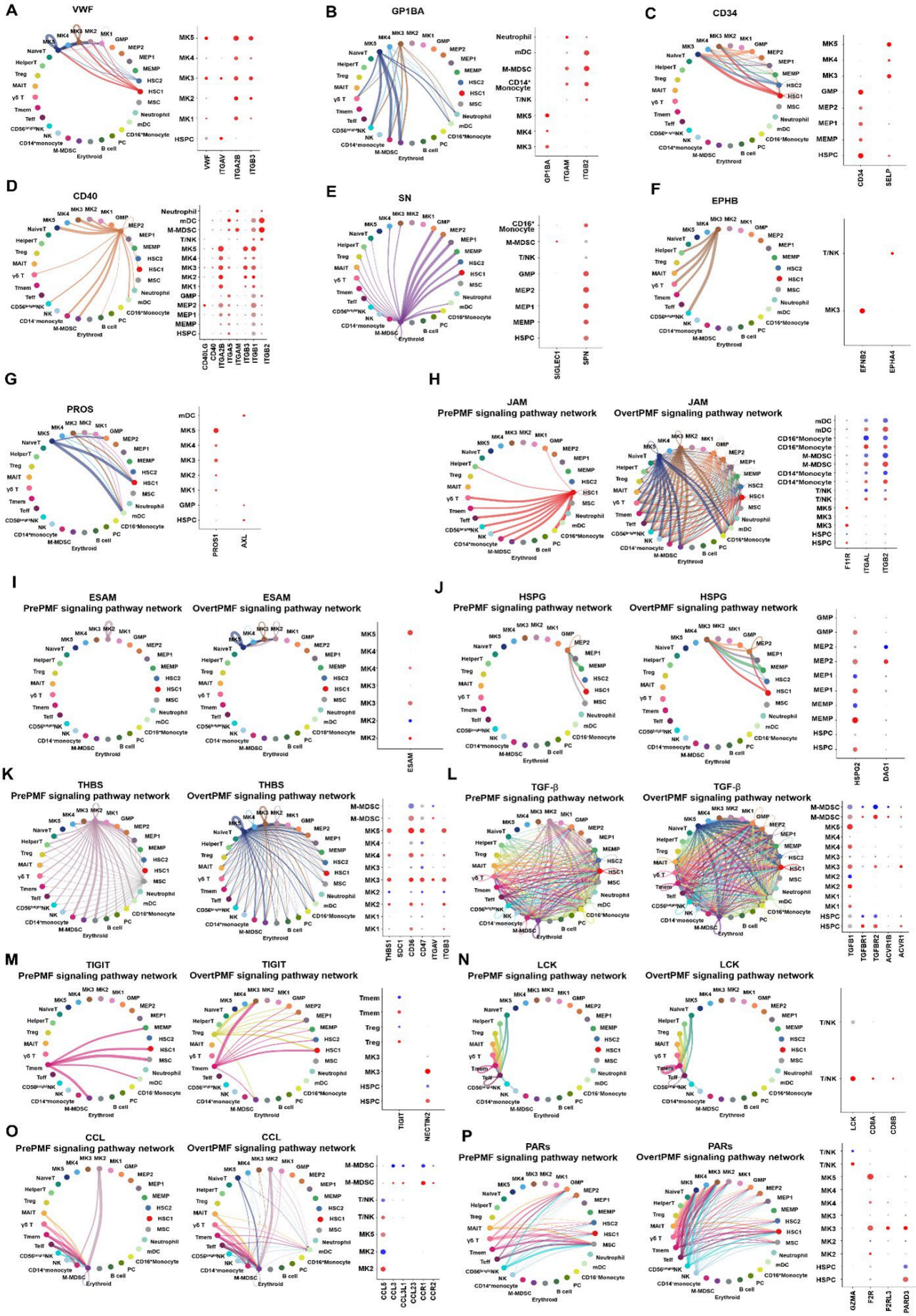
A
VWF
B
GP1BA
C
CD34
D
CD40
E
SN
F
EPHB
G
PROS
H
JAM
PrePMF signaling pathway network
JAM
OvertPMF signaling pathway network
I
ESAM
PrePMF signaling pathway network
ESAM
OvertPMF signaling pathway network
J
HSPG
PrePMF signaling pathway network
HSPG
OvertPMF signaling pathway network
K
THBS
PrePMF signaling pathway network
THBS
OvertPMF signaling pathway network
L
TGF-β
PrePMF signaling pathway network
TGF-β
OvertPMF signaling pathway network
M
TIGIT
PrePMF signaling pathway network
TIGIT
OvertPMF signaling pathway network
N
LCK
PrePMF signaling pathway network
LCK
OvertPMF signaling pathway network
O
CCL
PrePMF signaling pathway network
CCL
OvertPMF signaling pathway network
P
PARs
PrePMF signaling pathway network
PARs
OvertPMF signaling pathway network

Supplementary Fig. 6. Cell-cell communications enriched in overt PMF compared with pre-PMF. Circle plots (left panel) represent the inferred interaction pathways of (A) VWF, (B) GP1BA, (C) CD34, (D) CD40, (E) SN, (F), EPHB, and (G) PROS, which were exclusively identified in overt PMF, as well as those of (H) JAM, (I) ESAM, (J) HSPG, (K) THBS, (L) TGF-β, (M) TIGIT, (N) LCK, (O) CCL, and (P) PARs, identified in both pre-PMF and overt PMF. Edge width represents the communication probability (strength of the interactions) between cell populations. Edge colors are consistent with the signaling source. The expression of ligands and receptors for each signaling pathway in each cell subset from pre-PMF (blue) and overt PMF (red) is shown. Genes corresponding to ligands in each signaling pathway are indicated in bold. MK5 from pre-PMF was excluded due to a low number of cells.

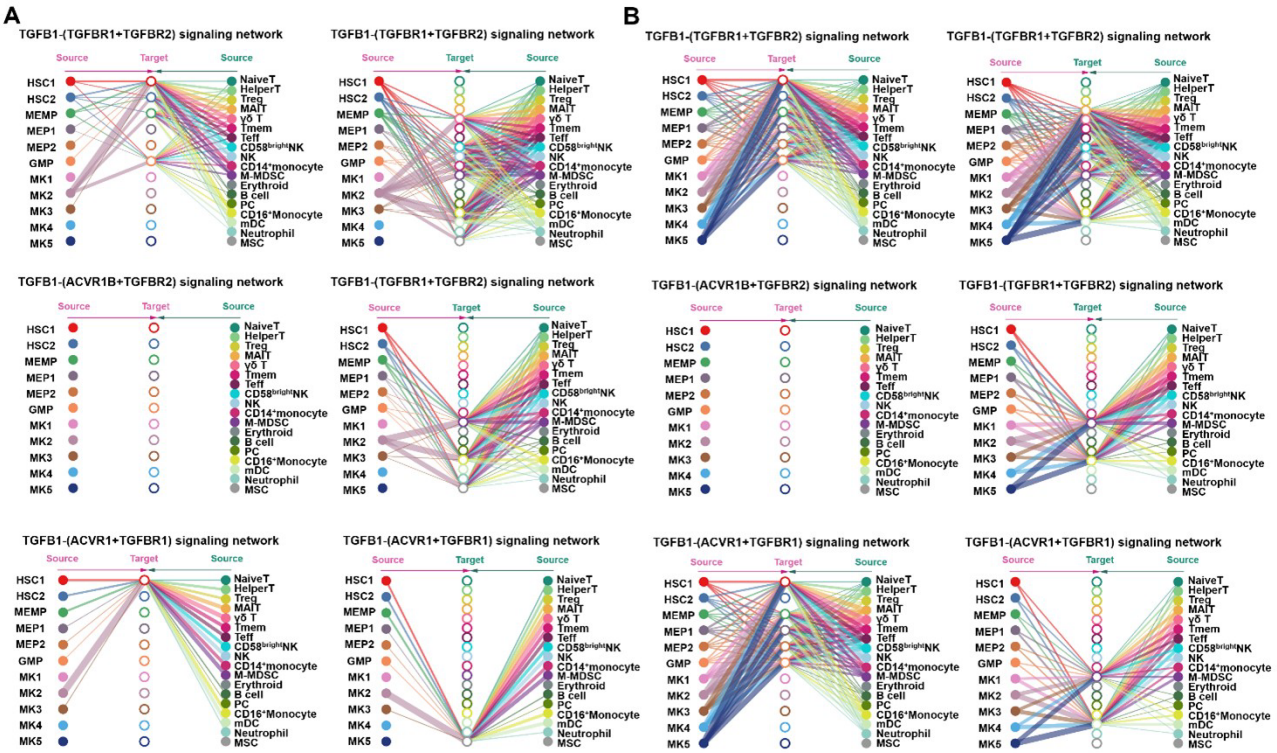

Supplementary Fig. 7. The inferred TGF-β signaling network. The inferred TGF-β signaling network from (A) pre-PMF and (B) overt PMF. Edge width represents the communication probability.

Supplementary Table 1. Significantly enriched genes in each BM cell subset.

The contents of Supplementary Table 1 are provided in a separate Excel file.

Supplementary Table 2. Pseudobulk DEGs of HSPC and MK between pre- and overt-PMFs

Subset	Gene	Avg_log2FC*	p_val**	p_val_adj**	pct.1§	pct.2§
HSC1	*ANXA2*	6.84	$9.1x10^{-09}$	$2.3x10^{-04}$	1.00	0.40
HSC1	*BACH2*	5.54	$1.3x10^{-08}$	$3.2x10^{-04}$	1.00	1.00
HSC1	*CPPED1*	5.46	$3.1x10^{-07}$	0.008	1.00	0.80
HSC1	*RAMP1*	6.62	$6.0x10^{-07}$	0.015	1.00	0.40
HSC1	*ZNF804B*	8.11	$8.0x10^{-07}$	0.021	1.00	0.60
HSC1	*ZNF98*	-1.16	$1.1x10^{-06}$	0.028	0.55	0.60
HSC1	*AXL*	7.47	$3.8x10^{-06}$	0.098	0.91	0.40
HSC1	*ANO2*	9.47	$6.7x10^{-06}$	0.173	0.91	0.40
MEP1	*SPATS2*	6.14	$2.2x10^{-09}$	$5.6x10^{-05}$	1.00	1.00
MEP1	*NAALADL2*	6.11	$3.2x10^{-08}$	$8.2x10^{-04}$	1.00	1.00
MEP1	*NLGN1*	12.90	$3.3x10^{-08}$	$8.6x10^{-04}$	1.00	0.00
MEP1	*PIEZO2*	6.71	$3.5x10^{-08}$	$9.1x10^{-04}$	1.00	0.75
MEP1	*LINC00511*	-1.41	$4.8x10^{-08}$	0.001	0.80	0.50
MEP1	*PLEKHA5*	5.25	$2.1x10^{-06}$	0.054	1.00	1.00
MEP1	*IMMP2L*	5.38	$2.9x10^{-06}$	0.073	1.00	1.00
MEP1	*HERC2*	5.87	$4.9x10^{-06}$	0.126	1.00	1.00
MK	*PRTN3*	-1.14	$1.1x10^{-11}$	$2.7x10^{-07}$	0.58	0.60
MK	*COL24A1*	10.46	$3.9x10^{-09}$	$1.0x10^{-04}$	0.92	0.20
MK	*FBXL7*	-1.61	$3.2x10^{-07}$	0.008	0.50	0.80
MK	*MAML3*	6.87	$3.4x10^{-07}$	0.009	1.00	1.00
MK	*KIAA1217*	-1.05	$3.7x10^{-07}$	0.010	0.58	1.00
MK	*SCPEP1*	1.78	$4.2x10^{-07}$	0.011	0.92	0.80
MK	*STXBP5*	6.75	$9.2x10^{-07}$	0.024	0.92	1.00
MK	*YES1*	7.07	$1.4x10^{-06}$	0.036	0.92	0.80
MK	*ARHGEF3*	6.69	$1.6x10^{-06}$	0.042	0.92	0.80
MK	*LTBP1*	8.17	$1.6x10^{-06}$	0.042	0.92	1.00
MK	*FAM30A*	6.73	$1.9x10^{-06}$	0.050	0.92	0.60
MK	*INPP4B*	7.73	$2.0x10^{-06}$	0.052	0.92	1.00
MK	*CXCL2*	8.67	$2.210x^{-06}$	0.057	0.83	0.40
MK	*GRB10*	7.46	$2.6x10^{-06}$	0.066	0.92	0.40
MK	*EFCAB13*	9.17	$3.5x10^{-06}$	0.089	0.83	0.60
MK	*UBASH3B*	7.34	$3.8x10^{-06}$	0.097	0.92	0.80
MK	*STEAP1B*	1.44	$4.9x10^{-06}$	0.126	0.83	1.00
MK	*GFPT1*	7.20	$6.5x10^{-06}$	0.166	0.92	0.60
MK	*SCFD2*	6.75	$6.7x10^{-06}$	0.173	0.92	1.00

*Log fold-change of the average expression between the selected cell populations and all other cell groups.

**p_val and p_val_adj represent the original *p*-value (unadjusted) and adjusted *p*-value based on Bonferroni correction using all features in the dataset, respectively.

§pct.1 and pct.2 represent the percentage of cells, where the feature is detected in the selected cell population and all other cell groups, respectively.

Supplemental References

1. Barbui T, Thiele J, Gisslinger H, et al. The 2016 WHO classification and diagnostic criteria for myeloproliferative neoplasms: document summary and in-depth discussion. Blood Cancer J. 2018;8(2):15.
2. Tefferi A. Primary myelofibrosis: 2021 update on diagnosis, risk-stratification and management. Am J Hematol. 2021;96(1):145-162.
3. Stuart T, Butler A, Hoffman P, et al. Comprehensive Integration of Single-Cell Data. Cell. 2019;177(7):1888-1902 e1821.
4. Wolock SL, Lopez R, Klein AM. Scrublet: Computational Identification of Cell Doublets in Single-Cell Transcriptomic Data. Cell Syst. 2019;8(4):281-291 e289.
5. Korsunsky I, Millard N, Fan J, et al. Fast, sensitive and accurate integration of single-cell data with Harmony. Nat Methods. 2019;16(12):1289-1296.
6. Aran D, Looney AP, Liu L, et al. Reference-based analysis of lung single-cell sequencing reveals a transitional profibrotic macrophage. Nat Immunol. 2019;20(2):163-172.
7. Andreatta M, Carmona SJ. UCell: Robust and scalable single-cell gene signature scoring. Comput Struct Biotechnol J. 2021;19(3796-3798.
8. Liberzon A, Subramanian A, Pinchback R, Thorvaldsdottir H, Tamayo P, Mesirov JP. Molecular signatures database (MSigDB) 3.0. Bioinformatics. 2011;27(12):1739-1740.
9. Jin S, Guerrero-Juarez CF, Zhang L, et al. Inference and analysis of cell-cell communication using CellChat. Nat Commun. 2021;12(1):1088.
10. Lannan KL, Sahler J, Kim N, et al. Breaking the mold: transcription factors in the anucleate platelet and platelet-derived microparticles. Front Immunol. 2015;6(48.
11. Nakamura-Ishizu A, Matsumura T, Stumpf PS, et al. Thrombopoietin Metabolically Primes Hematopoietic Stem Cells to Megakaryocyte-Lineage Differentiation. Cell Rep. 2018;25(7):1772-1785 e1776.
12. Poirault-Chassac S, Nivet-Antoine V, Houvert A, et al. Mitochondrial dynamics and reactive oxygen species initiate thrombopoiesis from mature megakaryocytes. Blood Adv. 2021;5(6):1706-1718.